AGU PUBLICATIONS

Journal of Advances in Modeling Earth Systems

RESEARCH ARTICLE
10.1002/2016MS000841

Redistribution of ice nuclei between cloud and rain droplets: Parameterization and application to deep convective clouds

M. Paukert[1,2], C. Hoose[1], and M. Simmel[3]

[1]Karlsruhe Institute of Technology, Institute of Meteorology and Climate Research, Karlsruhe, Germany, [2]Now at Pacific Northwest National Laboratory, Richland, Washington, USA, [3]Leibniz Institute for Tropospheric Research, Leipzig, Germany

Key Points:
- A parameterization scheme of aerosol-dependent raindrop freezing is presented
- Particle accumulation due to drop-drop collisions is considered explicitly
- Cloud glaciation with dust-mediated freezing is less efficient than with Bigg's approach

Correspondence to:
C. Hoose,
corinna.hoose@kit.edu

Citation:
Paukert, M., C. Hoose, and M. Simmel (2017), Redistribution of ice nuclei between cloud and rain droplets: Parameterization and application to deep convective clouds, *J. Adv. Model. Earth Syst.*, *9*, 514–535, doi:10.1002/2016MS000841.

Received 21 OCT 2016
Accepted 24 JAN 2017
Accepted article online 31 JAN 2017
Published online 21 FEB 2017

Abstract In model studies of aerosol-dependent immersion freezing in clouds, a common assumption is that each ice nucleating aerosol particle corresponds to exactly one cloud droplet. In contrast, the immersion freezing of larger drops—"rain"—is usually represented by a liquid volume-dependent approach, making the parameterizations of rain freezing independent of specific aerosol types and concentrations. This may lead to inconsistencies when aerosol effects on clouds and precipitation shall be investigated, since raindrops consist of the cloud droplets—and corresponding aerosol particles—that have been involved in drop-drop-collisions. Here we introduce an extension to a two-moment microphysical scheme in order to account explicitly for particle accumulation in raindrops by tracking the rates of selfcollection, autoconversion, and accretion. This provides a direct link between ice nuclei and the primary formation of large precipitating ice particles. A new parameterization scheme of drop freezing is presented to consider multiple ice nuclei within one drop and effective drop cooling rates. In our test cases of deep convective clouds, we find that at altitudes which are most relevant for immersion freezing, the majority of potential ice nuclei have been converted from cloud droplets into raindrops. Compared to the standard treatment of freezing in our model, the less efficient mineral dust-based freezing results in higher rainwater contents in the convective core, affecting both rain and hail precipitation. The aerosol-dependent treatment of rain freezing can reverse the signs of simulated precipitation sensitivities to ice nuclei perturbations.

1. Introduction

Aerosols have the potential to impact the atmospheric state via a number of different pathways [*Seinfeld and Pandis*, 2006], one of which is to mediate the primary formation of ice particles in clouds [*Pruppacher and Klett*, 1997]. In the mixed-phase regime between 0° and −36°C, immersion freezing is thought to be the most efficient way of heterogeneous ice nucleation [e.g., *Diehl and Mitra*, 2015; *Hiron and Flossmann*, 2015]. This mechanism is induced by a subset of aerosols (ice nuclei [IN]) which are immersed within a droplet [*Hoose and Möhler*, 2012]. By being cooled beyond a characteristic temperature, they act to trigger the phase change. A quantitative description of particle-specific ice nucleation efficiencies has been established only during the last years [*Hoose and Möhler*, 2012; *Vali*, 2014], providing the possibility to estimate the relative importance of different mechanisms and particle species.

The amount of ice particles present in clouds influences a multitude of cloud particle interactions in the mixed-phase regime. Consequently, the growth of large precipitating particles as well as the dissipation of small ones depends on the efficiency of droplet freezing. Overall, varying amounts of IN present in clouds are expected to modulate the evolution of clouds, surface precipitation, and radiative properties.

However, the relations between aerosol particles and resulting cloud properties pose challenges to the representation in atmospheric models, since the relevant mechanisms occur on the scales of molecules (nucleation) to millimeters (cloud condensate), while the resolved processes in numerical models range from tens of meters (large-eddy simulations) to tens of kilometers (global simulations). Therefore, subgrid parameterizations are necessary to calculate the influence of unresolved processes on grid-scale properties such as bulk ice contents within clouds. For example, *Johnson et al.* [2015] point out the specific role of drop freezing in their analyses of microphysical uncertainties in simulations of convective clouds. In climate

simulations, substantial uncertainty arises from the model representation of aerosol-cloud interactions and from the effects of ice nucleation in particular [*Boucher et al*., 2013]. *Bauer et al*. [2015] summarize that the improved representation of physics was among the key features to enhance the skill of numerical weather prediction in the past, and will remain a key in future.

In bulk models without explicit representation of aerosol, common parameterizations of immersion freezing follow the approach of *Bigg* [1953, hereinafter B53]. Based on droplet freezing experiments, accounting for the stochastic nature of nucleation, B53 enables the calculation of droplet freezing probabilities as a function of droplet volume. For an ensemble of raindrops with bulk mass density Q_r in kg m^{-3}, the rate of ice particle numbers originating from freezing rain is

$$\frac{\partial N_{ice,r}}{\partial t} = \frac{Q_r}{\rho_w}\, b\left(e^{-aT_c} - 1\right) \quad [\mathrm{m^{-3}\,s^{-1}}], \tag{1}$$

with temperature T_c in °C, $\rho_w = 1000\,\mathrm{kg\,m^{-3}}$. The parameters a and b are usually based on freezing experiments of collected rainwater [*Barklie and Gokhale*, 1959; *Wisner et al*., 1972].

While these parameters are assumed to be representative for any atmospheric conditions, further problems may arise with the quantification of ice nucleation activity of collected drops. These include (a) a significant amount of evaporating rain mass below cloud base during sedimentation (i.e., with a partly evaporation of drops, the relation between water mass and aerosol mass is not conserved) and (b) the scavenging of significant amounts of aerosol by the drops below cloud base when falling through a polluted, IN-containing atmospheric boundary layer ("washout") [e.g., *Garrett et al*., 2006; *Beheng and Herbert*, 1986]. Both evaporation and scavenging would tend to increase the aerosol content per liquid mass in the sampled rainwater, i.e., the drops within their cloudy environment may be less polluted than measured at ground levels. Applying such parameters to the in-cloud conditions as simulated by microphysical schemes may therefore result in overestimated freezing rates.

During past decades, attempts have been made to understand the physical nature of heterogeneous ice nucleation. A basic question is whether to interpret the immersion freezing mechanism as an analogon to homogeneous freezing (stochastic hypothesis), appreciating the fact that nucleation is an inherently stochastic phenomenon. Alternatively, to capture the variability of ice nucleating particles in an approximated way, we may attribute the freezing event to the properties of specific features located on the aerosol which would induce the freezing instantaneously (i.e., nonstochastically), given the appropriate thermodynamical conditions (singular hypothesis) [*Vali and Stansbury*, 1966].

With the formulation of equation (1) as commonly applied in models [e.g., *Khain et al*., 2000; *Seifert and Beheng*, 2006; *Morrison et al*., 2005; *Milbrandt and Yau*, 2005; *Lohmann et al*., 2001, and references therein], a drop ensemble which resides in an environment of constant temperature would be subject to close-to-constant freezing rates, and freezing may occur even during warming. Given enough time under these conditions—e.g., when low-speed updrafts balance the drop sedimentation velocity—the result will be a frozen fraction of droplets close to 1. While this formulation is intended to mimic the stochastic nature of nucleation (B53), later work concludes that a pure stochastic description was incompatible with the aerosol-dependent mechanism of immersion freezing [*Vali and Stansbury*, 1966; *Vali*, 1994]. With the stochastic component interpreted as a secondary effect, the singular hypothesis was shown to be a good approximation for heterogeneous freezing [*Vali*, 1994; *Welti et al*., 2012; *Vali*, 2014]. From this point of view, the freezing rate is expected to be close to zero in a constant-temperature drop environment, since the aerosol is activated in the moment of reaching its "characteristic freezing temperature" for the first time during its thermodynamical history. Consequently, with larger cooling rates (but identical local temperature), we would expect enhanced freezing rates, as more aerosols reach their characteristic freezing temperature per time interval, as confirmed by *Vali and Stansbury* [1966].

When modeling studies aim to investigate ice nucleation impacts on cloud properties, often the number of activated IN is directly translated into the number of freezing cloud droplets. In that case, with none of the ice nucleating particles being attributed to raindrops, immersion freezing of rain is still parameterized as an aerosol-independent process (equation (1)). This may be appropriate to simulate clouds with low droplet collision activities and no significant warm rain formation. Otherwise, such a treatment has the potential to substantially underestimate the simulated sensitivity of clouds to ice nuclei [*Khain et al*., 2015], since larger

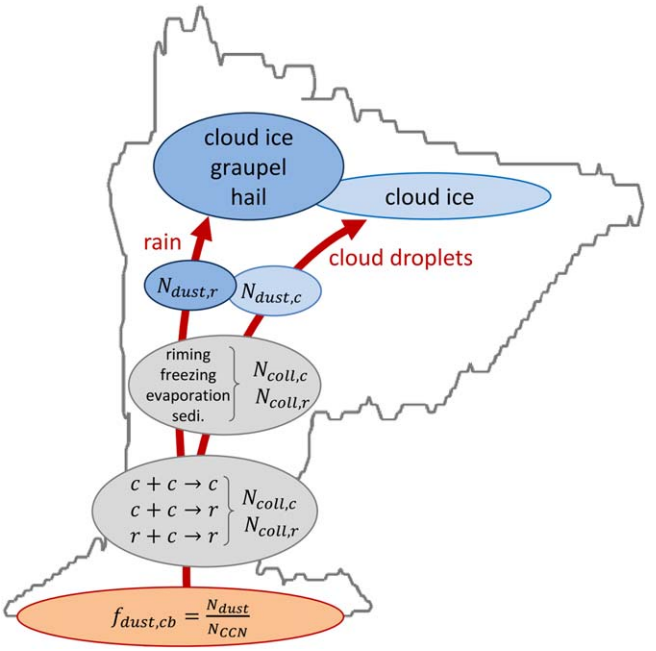

Figure 1. Schematic of the processes involved in our implementation of immersion freezing. Combined with the mineral dust fraction at cloud base $(f_{dust,cb})$, the number of collected CCN in cloud and raindrops $(N_{coll,c/r})$ yield an estimate for the dust particles immersed in both drop classes $(N_{dust,c/r})$. Consistent with the implementation of *Blahak* [2008], frozen rain results in cloud ice, graupel and hail particles. Droplet collisions among cloud droplets (c) and rain (r) are parameterized following [*Seifert and Beheng*, 2006]. The outer boundaries indicate the edges of a simulated supercell from the side view after 70 min (precipitating particles excluded from the boundaries).

drops make more important contributions to rain formation than smaller ones, even when the ice phase is involved as an intermediate step via riming. Early evidence for the role of large freezing drops to initiate large ice particles, followed by riming and precipitation formation was found by *Koenig* [1963] and *Braham* [1964]. *Phillips et al*. [2001] find a paramount influence of large freezing drops on cloud glaciation, and *Taylor et al*. [2016] report significant contributions of drizzle and raindrop freezing to the formation of large ice.

Generally, the freezing probability of a drop depends on the amount and physical properties of the potential IN immersed in it. We can expect that the properties of the immersed particles are highly case-specific, and a variability along the microphysical trajectory of the drop. Besides the ambient aerosol particle population, it is the rates of collision and coalescence which determine the amount of accumulated particles within large drops. In a simplified approach, *Saleeby and van den Heever* [2013] treat this transfer of immersed aerosol between hydrometeor categories as proportional to the transfer in condensate mass. To date, only some spectral microphysical schemes account for the redistribution of aerosol among the cloud particle classes without invoking such ad hoc assumptions on the distribution of the aerosol mass within the hydrometeor size distribution [e.g., *Diehl and Mitra*, 2015]. However, these are computationally demanding and become applicable to large three-dimensional domains only slowly, particularly when sensitivity studies involve numerous simulations.

In this work, a two-moment microphysical model [*Seifert and Beheng*, 2006] is extended to track the microphysical history of raindrops explicitly. A suggestion similar to the basic ideas of this study was made by *Phillips et al*. [2008], but to our knowledge, no model implementation exists to date. Based on the ideas of the singular hypothesis, a freezing parameterization is derived for mineral dust particles [*Niemand et al*., 2012], considering multiple IN per drop as well as the dependencies on updraft speeds and drop sedimentation.

In the following, an overview of the model implementations will be presented (section 2). In section 3 we will validate the assumptions made for the model extensions by applying a two-dimensional bin microphysics parcel model. Finally, section 4 will show the resulting redistribution of dust between cloud and raindrops in simulations of deep convective clouds, and a comparison of cloud properties as a result of the default model treatment and our new method.

2. Model Implementation

An overview of the processes involved in our implementation is given in Figure 1. After activation of cloud condensation nuclei (CCN) at cloud base, each cloud droplet contains exactly one CCN. Subsequently, the processes of cloud droplet selfcollection, autoconversion, and accretion of cloud droplets by raindrops will lead to collisional droplet growth. In the model, these processes are parameterized according to *Seifert and*

Beheng [2001] and *Seifert and Beheng* [2006]. At the same time, the collisional growth of drops results in particle accumulation.

We account for the accumulation of CCN by tracking the drop collision rates, which yields the bulk number of CCN immersed in cloud droplets ($N_{coll,c}$) and in raindrops ($N_{coll,r}$). Depletion of immersed aerosols results from droplet removal mechanisms during riming, freezing, and complete drop evaporation. For $N_{coll,r}$, the sedimentation of rain is considered. Both $N_{coll,c}$ and $N_{coll,r}$ are represented by tracers in the model, i.e., they are subject to grid-scale advection and turbulent diffusion.

Combining the information of CCN per drop with the fraction of ice nuclei during CCN activation at cloud base ($f_{dust,cb}$) yields the number of potential IN immersed in cloud droplets ($N_{dust,c}$) and raindrops ($N_{dust,r}$) relevant for freezing. The temperature dependence of ice nucleation is parameterized according to *Niemand et al*. [2012, hereinafter N12]. We identify the implementation of N12 for cloud and raindrop freezing presented in this study with "P17."

Throughout this study, our definition of "rain" drops contains all drop sizes larger than 80 μm in diameter, consistent with an assumption in our microphysical scheme [*Seifert and Beheng*, 2006]. "Cloud droplets" have diameters less than 80 μm. We note that "drizzle" drops with diameters smaller than 500 μm as defined by the American Meteorological Society are contained in the rain category, as common in bulk microphysical schemes.

2.1. Particle Accumulation in Cloud and Raindrops

$N_{coll,c/r}$ can be interpreted as the number concentration of CCN incorporated into the droplets by collisions. By definition, these numbers only account for collected CCN, i.e., in a population of cloud droplets without the presence of selfcollection $N_{coll,c}=0$. Since at least one event of autoconversion must be present prior to the existence of a raindrop, $N_{coll,r} \geq 2\,N_r$ in presence of rain, where N_r is the bulk number concentration of raindrops.

Since raindrops consist of the cloud droplets that were collected during collisions, our basic assumption is that the number of collected particles per single raindrop is proportional to the drop liquid mass. This is relevant for the budgets described in the following and will be tested and largely confirmed in section 3. We express the proportionality of particle number to drop mass through r_{CCN}, defined as $\frac{N_{coll,r}}{Q_r}$ and assumed to be independent of the raindrop size.

In the following, the budgeting of $N_{coll,c/r}$ is described. The processes involve drop-drop-collisions on the one hand, and liquid-depleting mechanisms on the other hand.

2.1.1. Selfcollection, Autoconversion, and Accretion

With the cloud droplet number N_c, we define the mean number of collected particles in cloud droplets as

$$\lambda_c = \frac{N_{coll,c}}{N_c} \geq 0. \tag{2}$$

As indicated above, the cloud droplet population consists of two types of droplets: (a) "pristine droplets" with one CCN per droplet ($\lambda_c=0$) and (b) a typically small subset of "nonpristine" droplets with more than one CCN per droplet ($\lambda_c > 0$).

During selfcollection, the collision of two cloud droplets results in one cloud droplet. The accumulation of $N_{coll,c}$ may be the result of collisions between both pristine and nonpristine droplets. The rate of collected CCN is therefore

$$\mathrm{d}N_{coll,c} = -\mathrm{d}N_{c,sc}, \tag{3}$$

where $\mathrm{d}N_{c,sc}$ is the parameterized selfcollection rate of cloud droplets [*Seifert and Beheng*, 2001, equation (A9)]. The sum on the right-hand side corresponds to the mean number of total CCN per cloud droplet.

During autoconversion, two cloud droplets form one raindrop. The budget equations for collected CCN in cloud and raindrops are

$$\mathrm{d}N_{coll,r} = -\,\mathrm{d}N_{c,au}\,(\lambda_c+1), \tag{4}$$

$$dN_{coll,c} = dN_{c,au}\,\lambda_c \quad , \tag{5}$$

with the rate of cloud droplet numbers due to autoconversion $dN_{c,au}$ [*Seifert and Beheng*, 2001, equation (A5)]. The rates of accretion are tracked analogously, with

$$dN_{coll,r} = -dN_{c,acc}\,(\lambda_c + 1), \tag{6}$$

$$dN_{coll,c} = dN_{c,acc}\,\lambda_c \quad , \tag{7}$$

and $dN_{c,acc}$ being the number change rate of cloud droplets due to accretion [*Seifert and Beheng*, 2001, equation (A6)].

2.1.2. Budgeting of Sinks Other Than Drop-Drop Collisions

Sinks for both $N_{coll,c}$ and $N_{coll,r}$ are given by processes which consume liquid droplets completely at a time, such as droplet freezing, collisions with ice particles, and droplet evaporation.

Because of the different nature of the growth mechanisms of cloud and raindrops $N_{coll,c}$ and $N_{coll,r}$ are treated differently. The dominant condensational growth of cloud droplets implies that nearly all droplets contain only one particle, independent of the droplet mass. Thus, during cloud droplet removal (dN_c), the depletion of $N_{coll,c}$ scales with the mean number of CCN per droplet, i.e.,

$$dN_{coll,c} = dN_c\,\lambda_c. \tag{8}$$

In contrast, raindrop growth is dominated by drop-drop-collisions, with each of the collected cloud droplets corresponding to approximately one CCN. Thus, it is assumed that the bulk content of collected particles in rain, $N_{coll,r}$, is distributed homogeneously among the raindrop mass, and the number of CCN for each drop is proportional to the drop mass, independent of the drop sizes throughout the size distribution. During raindrop removal, the depletion of $N_{coll,r}$ is therefore proportional to the depleted rain mass dQ_r during freezing and riming of raindrops. Thus, the CCN number density per rain mass is conserved. We define $x_{coll,r}$ to be the mean rain mass attributed to exactly one CCN according to the bulk properties of rain, i.e.,

$$x_{coll,r} = \frac{Q_r}{N_{coll,r}}. \tag{9}$$

The sink of N_{coll} during homogeneous freezing and riming with mass changes dQ_r are then

$$dN_{coll,r} = \frac{dQ_r}{x_{coll,r}}. \tag{10}$$

Heterogeneous freezing is not a sink for N_{coll} because the number of IN as parameterized by equation (15) is based on all dust particles within both unfrozen and heterogeneously frozen drops. Therefore, a strict interpretation as CCN per liquid mass is not valid any longer when heterogeneous freezing begins to influence the budget.

For evaporating raindrops, changes of drop number concentrations are parameterized as a function of evaporating mass and the shape of the size distribution [*Seifert*, 2008, equations (22) and (23)]. The budget of $N_{coll,r}$ is affected only by the subsample of drops which evaporate completely. Since the rate of evaporating rain mass contains also the incomplete evaporation of larger drops, dQ_r cannot be used here. Instead, because the change of raindrop number is defined by the number of drops becoming smaller than 80 μm [*Seifert*, 2008], we use the parameterized number of evaporating drops, multiplied the single-drop mass (x_{80}) corresponding to a size of $D = 80$ μm.

$$dN_{coll,r} = \frac{dN_{r,eva} \cdot x_{80}}{x_{coll,r}}. \tag{11}$$

Sedimentation of raindrops acts as a transport mechanism of $N_{coll,r}$. Sedimentation fluxes result in a transport of rain mass into the grid box at its upper boundary ($dQ_{r,in}$), and transport out of the box at its lower boundary ($dQ_{r,out}$), with $dQ_{r,in}$ having the properties of the overlying level. Analogously to the rain mass change as a result of the sedimentation flux divergence, the budget of collected particles is determined by the difference of incoming and outgoing collected particles, each of which is calculated from $dQ_{r,in}$ and $dQ_{r,out}$.

$$dN_{coll,r,in/out} = \frac{dQ_{r,in/out}}{x_{coll,r,in/out}}. \quad (12)$$

In cloud-free regions, both $N_{coll,c}$ and $N_{coll,r}$ are reset to zero.

2.2. Cloud Base Fraction of Potential Ice Nuclei

In order to determine the number of a specific aerosol species immersed within the drops ($N_{dust,c/r}$ for mineral dust in cloud and raindrops, respectively), we relate the previously tracked CCN to the fraction of the corresponding aerosols at cloud base ($f_{dust,cb}$)

$$N_{dust,c} = (N_c + N_{coll,c})\, f_{dust,cb} \quad \left[\mathrm{m}^{-3}\right], \quad (13)$$

$$N_{dust,r} = N_{coll,r}\, f_{dust,cb} \quad \left[\mathrm{m}^{-3}\right]. \quad (14)$$

The dust fraction should be determined during the calculation of CCN activation, whenever activation occurs in the model in different locations. Accordingly, $f_{dust,cb}$ should be represented by a tracer which is subject to advection and turbulent diffusion.

A simplified approach is used throughout this study, assuming a constant $f_{dust,cb}$ within the cloud. It is representative for the boundary layer concentrations of aerosols available for droplet activation, and the mineral dust concentration. This simplification is used because of several sources of uncertainty for calculating $f_{dust,cb}$ in the current model setup (see also section 4.1). While here we parameterize CCN activation according to *Segal and Khain* [2006], a composition-dependent approach with prognostic aerosols in the model should be used to calculate $f_{dust,cb}$ explicitly.

We note that the relation stated in equation (14) represents a simplified estimation of the true amount of rain-immersed dust; for example, the relatively large coarse mode dust may have formed larger initial droplets compared to average CCN sizes and thus may have collided preferentially with other droplets. Therefore, the true history of the IN-containing drops can be different from average drop properties to some extent.

2.3. Freezing of Raindrops

According to the idea of "active sites" on an ice-nucleating particle, droplet freezing probabilities depend on the particle surface area [e.g., *Murray et al*., 2012], and therefore the number of mineral dust particles immersed within the drops (equation (14)).

A temperature-dependent fraction of $N_{dust,r}$ will be activated as IN. We assume the mineral dust to be composed of a lognormal distribution, $n_{dust,r}(D)$. Integration over the mineral dust size distribution yields the total number of activated IN at a specific temperature

$$N_{IN,r} = \int n_{dust,r}(D) \left(1 - e^{-n_s \pi D^2}\right) dD \quad \left[\mathrm{m}^{-3}\right]. \quad (15)$$

The particle-specific temperature dependence of ice nucleation is parameterized according to N12 with the surface site density

$$n_s(T_c) = e^{-a_{N12} T_c + b_{N12}} \quad \left[\mathrm{m}^{-2}\right]. \quad (16)$$

with temperature T_c in °C and fit parameters a_{N12} and b_{N12}.

2.3.1. Monodisperse Drop Ensemble

First we consider a monodisperse sample of raindrops with known $N_{IN,r}$ according to equation (15). For this equal-sized drop ensemble, we can assume the particles to be Poisson-distributed among the drops to estimate the freezing probabilities [*Vali*, 1971; *Hartmann et al*., 2013]. Therefore, with the mean number of activated particles per drop

$$\lambda_{IN} = \frac{N_{IN,r}}{N_r}, \quad (17)$$

the probability of finding k IN immersed in one drop is

$$P(X=k)=\frac{\lambda_{IN}^{k}}{k!}e^{-\lambda_{IN}}. \tag{18}$$

Freezing of a drop is triggered with at least one activated IN being immersed in it, and no freezing will occur with $k=0$. Therefore, the probability for the freezing of a drop is $P(X>0)=1-P(X=0)=1-e^{-\lambda_{IN}}$. For an ensemble of drops, this is equal to the freezing fraction, and the number of frozen raindrops is

$$N_{ice,r}=N_r\left(1-e^{-\lambda_{IN}}\right). \tag{19}$$

Equation (19) is not directly applicable in models because during the model time integration the rate of freezing is required in each time step. In case of cloud droplet freezing, the rate can be reconstructed by making assumptions about previously activated aerosol particles, most easily by assuming that preexisting cloud ice and snow number densities correspond to activated aerosol particles (SB06), or by introducing specific tracers for activated IN in the model [*Paukert and Hoose*, 2014]. Such methods are particularly problematic for raindrops because of nonnegligible sedimentation effects not only of rain, but also of sedimenting large ice particles. Also explicit tracking activated IN may result in inconsistencies because of sedimentation. For these reasons, we avoid the use equation (19) in the model, but derive a rate equation instead.

The freezing rate is calculated from the time derivative of equation (19), where λ_{IN} is a function of $n_s(T)$. In particular, the freezing rate depends on the steepness of $n_s(T)$ and the effective cooling rate of the drops. In addition to the updraft speed, the effect of drop sedimentation can be considered easily, resulting in a decreased effective cooling rate for sedimenting drops and a reduced freezing rate. The treatment implies that heterogeneous freezing occurs only for drops which move upward, i.e., where $(w-v_{sed})>0$ with v_{sed} being positive downward. From equation (19) we obtain

$$\frac{\partial N_{ice,r}}{\partial t}=-e^{-\lambda_{IN}}\,n_s\,a_{N12}\,(w-v_{sed})\,\frac{\partial T}{\partial z}\int\pi D^2 n_{dust,r}(D)\,e^{-n_s\pi D^2}\,\mathrm{d}D, \tag{20}$$

where a_{N12} is the fit parameter belonging to the parameterization of $n_s(T)$ (equation (16)). $\frac{\partial T}{\partial z}$ is the moist adiabatic temperature gradient, and D is the diameter of dust particles. Note that at this point we are still considering a monodisperse drop ensemble, with v_{sed} being the individual drop sedimentation velocity. In the model, equation (20) is applied to multiple drop sizes, as described below in this section. The integral is applied to the bin-resolved, prescribed dust size distribution in the model.

A higher degree of approximation is derived for comparison (see Figure 2), using the mean dust surface area, $\bar{S}_{dust,r}=\frac{S_{dust,r}}{N_{dust,r}}$, to calculate the total number of activated dust particles.

$$\lambda_{IN}=\frac{N_{IN}}{N_r}=\frac{N_{dust,r}\left(1-e^{-n_s\bar{S}_{dust,r}}\right)}{N_r}, \tag{21}$$

$$\frac{\partial N_{ice,r}}{\partial t}=-e^{-\lambda_{IN}}\,n_s\,a_{N12}\,(w-v_{sed})\,\frac{\partial T}{\partial z}N_{dust,r}\,\bar{S}_{dust,r}\,e^{-n_s\bar{S}_{dust,r}}. \tag{22}$$

2.3.2. Polydisperse Drop Ensemble

In the preceding calculations, we assumed a monodisperse sample of raindrops in order to derive the number freezing rate under consideration of multiple activated IN per drop. To account for the generalized gamma distributions as assumed in our microphysics scheme [*Seifert and Beheng*, 2006], our approach is as follows.

In a drop size dependent calculation, λ_{IN} is a function of drop mass (or volume), i.e., larger raindrops will have higher freezing probabilities than small raindrops. Therefore, we solve equation (20) in the model for several raindrop sizes, i.e., the spectrum resulting from the bulk rain properties is subdivided into eight drop size intervals ("PSD splitting" hereafter). The upper boundaries of the intervals are defined at masses (x_{ubd}) corresponding to the diameters of 60, 125, 250, 500, 600, 1250, and 1500 μm. In order to calculate q_r and n_r contained in each one of the size intervals, we integrate from 0 to each one of the upper boundaries (x_{ubd}).

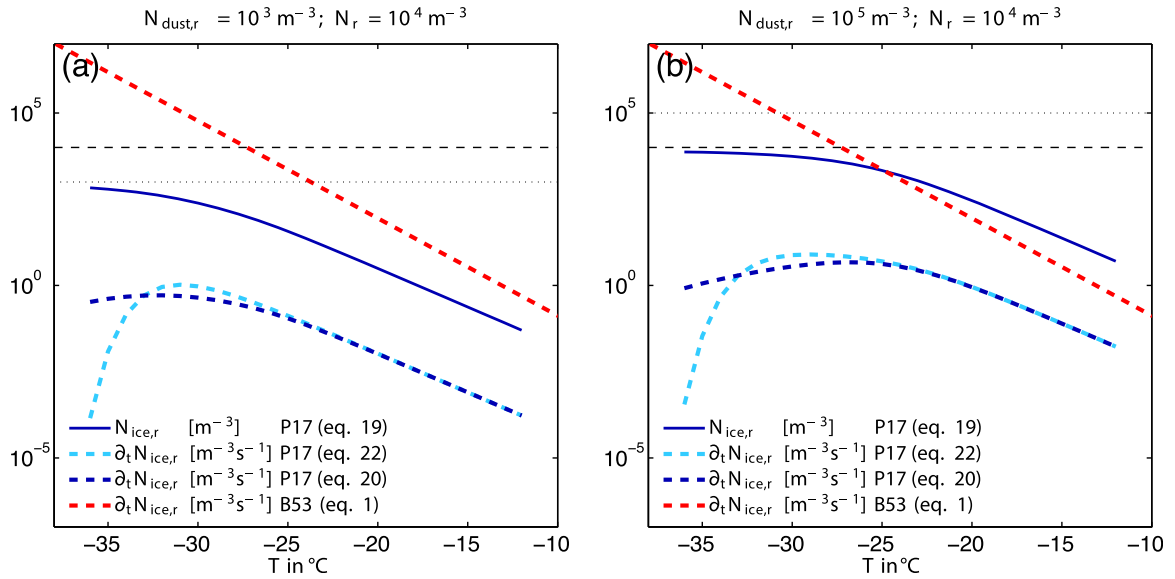

Figure 2. Total ice number densities (full lines) and freezing rates (dashed lines) resulting from different approaches, with (a) $N_{dust,r}=10^3\ \mathrm{m}^{-3}$ and (b) $N_{dust,r}=10^5\ \mathrm{m}^{-3}$. Horizontal dashed lines indicate $N_r=10^4\ \mathrm{m}^{-3}$ in both cases, and horizontal dotted lines indicate $N_{dust,r}$. The examples are based on $w=1\ \mathrm{m\,s}^{-1}$ and $Q_r=1\ \mathrm{g\,m}^{-3}$. The COSMO model makes use of the equation (20) (dark blue), while the default model implementation (B53, red dashed) yields rates which are higher by several orders of magnitude.

$$n_r=\frac{A}{\mu B^{\frac{\nu+1}{\mu}}}\,\gamma\left(\frac{\nu+1}{\mu},B\,x_{ubd}^{\mu}\right), \tag{23}$$

$$q_r=\frac{A}{\mu B^{\frac{\nu+2}{\mu}}}\,\gamma\left(\frac{\nu+2}{\mu},B\,x_{ubd}^{\mu}\right), \tag{24}$$

$$B=\left[\frac{\Gamma\left(\frac{\nu+1}{\mu}\right)}{\Gamma\left(\frac{\nu+2}{\mu}\right)}\frac{Q_r}{N_r}\right]^{-\mu}, \tag{25}$$

$$A=\frac{\mu N_r B^{\frac{\nu+1}{\mu}}}{\Gamma\left(\frac{\nu+1}{\mu}\right)}. \tag{26}$$

Small letters indicate the number and mass of rain contained per interval, and capital letters indicate bulk properties. Subtraction of smaller categories from larger ones yields the concentrations within a single interval. The concentration of dust particles per interval results from the rain mass per interval q_r, the number of CCN per liquid mass (section 2.1) and the dust fraction at cloud base (section 2.2)

$$n_{dust,r}=q_r\,r_{CCN}\,f_{dust,cb}. \tag{27}$$

Applying these properties to equation (20) yields the number of frozen drops per size interval. The corresponding mass rate results from multiplication by the mean drop mass of the corresponding interval.

Freezing raindrops contribute to the formation of cloud ice, graupel, and hail particles [*Blahak*, 2008]. By default, the drop distribution is divided into three size ranges, up to 500 μm for cloud ice, from 500 to 1250 μm for graupel, and from 1250 μm onward for hail. PSD splitting avoids the need for piecewise analytical integration over the rain PSD by applying equation (20) to a small number of size intervals. The subsequent attribution of frozen particles to the three ice particle classes is straight-forward. In the current implementation, the size spectrum corresponding to cloud ice is subdivided into four intervals, and graupel and hail-forming drops are subdivided into two intervals each.

Hail-forming drops have smaller effective cooling rates than cloud ice-forming drops. Size-specific sedimentation is calculated consistently with the model assumptions depending on the drop mass and a correction factor for air density.

For the sake of simplification, we can think of disregarding the PSD splitting, i.e., treating the whole rain size distribution at once. In this case, the model implementation is slightly different: the freezing rates of the whole spectrum are calculated first, and splitting of the rates into the three particle classes of cloud ice, graupel, and hail is performed subsequently. In sensitivity tests with intermediate dust concentrations (section 4.3), the effect of PSD splitting as compared to the simpler method will be discussed. It will be shown that accounting for the drop size dependencies has the largest impact on hail formation, while cloud ice and graupel are influenced to a minor extent.

2.3.3. Freezing Rates

In Figure 2, we compare the solution for parameterized freezing rates (equation (20)) with the existing model implementation for freezing rain according to *Bigg* [1953, equation (1)]. The calculations are based on 10^3 m^{-3} (Figure 2a) and 10^5 m^{-3} (Figure 2b) dust particles contained in the raindrop spectrum, consisting of 10^4 m^{-3} drops which are lifted with a vertical velocity of 1 $m\,s^{-1}$, and a rain mass density of 1 $g\,m^{-3}$. The drop spectrum is defined consistent with the COSMO model.

In Figure 2, the total ice number ($N_{ice,r}$) is shown by full lines as a function of temperature. With decreasing temperature, the activated fraction of dust particles approaches 1, and depending on the specific approach, most of the drops freeze. The calculation according to equation (19) (full dark blue line) results in a plateau region with quasi-constant frozen drop numbers in the coldest portion, and the parameterized rate decreases accordingly (dashed dark blue line).

Although it may be counterintuitive to find decreasing freezing rates at colder temperatures, this is expected for two reasons, as shown in Figures 2a and 2b. On one hand, $N_{ice,r}$ approaches the limit given by $N_{dust,r}$ (Figure 2a, horizontal dotted line). Even with homogeneously distributed dust particles in the drops, $N_{ice,r}$ cannot exceed $N_{dust,r}$ when considering immersion freezing only. On the other hand, with $N_{dust,r} > N_r$ (Figure 2b), it is clear that $N_{ice,r}$ is limited by N_r. In both cases (a) and (b), the rates must decrease necessarily in order not to exceed the limits given by $N_{dust,r}$ and N_r. It is also evident in Figure 2 that even with an activated dust fraction close to 1 at the coldest temperatures, $N_{ice,r}$ is smaller than $N_{dust,r}$ because the calculation allows for multiple IN being immersed in large drops.

The calculations based on $\bar{S}_{dust,r}$ (light blue lines) tend to overestimate ice formation in the transition temperature regime before the plateau is reached. Nevertheless, the differences betweens equations (20) and (22) are small compared to the deviation from equation (1) (B53).

For comparison, the B53-based rate is indicated by the red dashed line. It is independent of the vertical velocity, i.e., with higher updraft speeds (here: 1 $m\,s^{-1}$), P17 rates would become more similar to B53. In section 4.3 it will be shown that also with $N_{dust}=10^6$ m^{-3} and in strong convection, P17 immersion freezing is less efficient than B53.

3. SPECS Parcel Model Simulations

Here we seek to validate the assumption made in sections 2.1 and 2.3 that the number of collected particles within the raindrop size spectrum is proportional to raindrop mass. We investigate this by applying a bin microphysical model to simulate droplet collisions in a detailed manner. In the two-dimensional bin microphysics version of the SPECS (spectral cloud microphysics) model [*Simmel et al*., 2002; *Simmel and Wurzler*, 2006] as used here, the drop spectrum is divided into 132 bins (first dimension), while every drop size interval is binned into 180 aerosol mass categories (second dimension). By solving the stochastic collection equation numerically, the SPECS model yields the evolution of drop spectra as well as CCN mass contents within the droplets. Furthermore, supersaturation and condensational growth are predicted. The notation of cloud and raindrops is used consistently with the previous sections, and x is the single-particle droplet mass in kg.

For the budgeting of collected aerosol particles in raindrops as well as for raindrop immersion freezing (section 2), we assumed that the number of CCN per drop mass (r_{CCN}) is constant throughout the raindrop spectrum, i.e., for drops with $D > 80$ μm: $\frac{N_{CCN}(x)}{x} = r_{CCN} = const$.

This approximation is expected to be valid in case that (a) the raindrop growth is dominated by autoconversion and accretion rather than by condensation and (b) the cloud droplets converted to rain have a narrow range of r_{CCN}. Otherwise, if a broader range of r_{CCN} is involved, the assumption will still be valid if the

stochastic behavior of the collisions acts to mask the variability, i.e., the distribution of multiple r_{CCN} of cloud droplets contained within one raindrop would yield the same average r_{CCN} for all raindrops.

Cloud droplets are expected to grow mainly from condensation because the selfcollection of cloud droplets is relatively inefficient (see Figure 5). Thus, with the average aerosol particle number per cloud droplet being close to 1, $r_{CCN} \approx x^{-1}$, and condition (b) corresponds to the requirement that only a narrow size range of cloud droplets is favored for the conversion to rain. The condition is not fulfilled if different raindrop sizes prefer to collect cloud droplets of considerably different sizes.

Given the fulfilled conditions (a) and (b) as defined above, subsequent collisions among raindrops increase the number of CCN per drop, with r_{CCN} being conserved throughout the rain spectrum.

3.1. SPECS Model Setup

The box model is driven by a constant ascent of 2 m s^{-1}, with an initial temperature of 263 K and 99% relative humidity with respect to water. This updraft speed provides enough time for the narrow spectrum to yield large raindrops in the end of the simulations (3000 s, corresponding to 8 km altitude).

In a sensitivity simulation, the effect of entrainment and detrainment of aerosol particles and drops is considered by parameterizing the mixing between the parcel and its environment depending on the vertical velocity and parcel size [*Simmel et al.*, 2005]. Assuming the environmental aerosol mixing ratios to be equal to the initial state of the parcel (see below), aerosol particles are mixed in both directions, and droplets are detrained. Overall, this modifies the supersaturation within the parcel and enables CCN activation above the cloud base due to the continuous flux of freshly entrained aerosol.

The initial aerosol size distribution is unimodal and very narrow: Our primary interest is the number of CCN per drop depending on drop size, while the model tracks the mass of CCN rather than numbers of CCN. During time integration, the drop collisions act to redistribute the masses of liquid and aerosols in the two-dimensional spectrum, thereby losing any information about the underlying particle spectrum associated with the accumulated mass per bin. Since we want to relate aerosol mass to aerosol number concentrations, the initial aerosol spectrum is quasi-monodisperse in our simulations, with a concentration of 283 cm^{-3}, a mode diameter of 50 nm and a standard deviation of 1.01. Therefore, we can infer the aerosol number from the simulated aerosol mass per bin, using the mean aerosol mass during initialization.

In order to focus on the effect of droplet collisions, freezing and ice microphysics are excluded. Unactivated, interstitial aerosol particles are enabled to interact with droplets, and may be incorporated in the droplets as a result of scavenging. By disabling scavenging, it was confirmed that its effect on r_{CCN} is negligible for this study (not shown). Breakup of large drops is disregarded for the simulations which are analyzed in the following, although the effect is rather inefficient with the narrow initial spectrum and limited time for growth.

3.2. SPECS Results and Discussion

Figure 3 shows the temporal evolution of the parcel-integrated number concentrations, with and without entrainment. The time evolution of total particles is given by the sum of unactivated aerosol ($D < 1$ μm) and droplets ($D > 1$ μm). Without entrainment (Figure 3a), their concentration is basically equal to the droplet concentrations, except that droplets larger than 10 μm need some time to grow by condensation initially. The primary reduction of particle concentrations is attributed to the expanding parcel size with height. After 2500 s, the majority of small droplets has been converted to rain, and the total droplet number decreases quickly.

With entrainment included (Figure 3b), the total number concentration (red dashed) and the droplet number concentrations diverge because of the continuous entrainment of aerosol on the one hand, and detrainment of droplets on the other hand. Because of smaller droplet numbers, the supersaturation is higher and increases faster when entrainment is included (not shown). At 1800 s, this enables the activation of new CCN (full red line in Figure 3b1). These "secondary" droplets grow beyond 5 μm within 100 s (light blue line), but the condensational growth is not efficient enough to yield sizes larger than 10 μm (dark blue line). Another smaller amount of CCN is activated after 2900 s when the supersaturation exceeds 0.5%. Overall, the activation events above cloud base result in a bimodal size distribution of droplets, with a slowly growing mode diameter of the smaller mode with time ($D < 10$ μm; not shown).

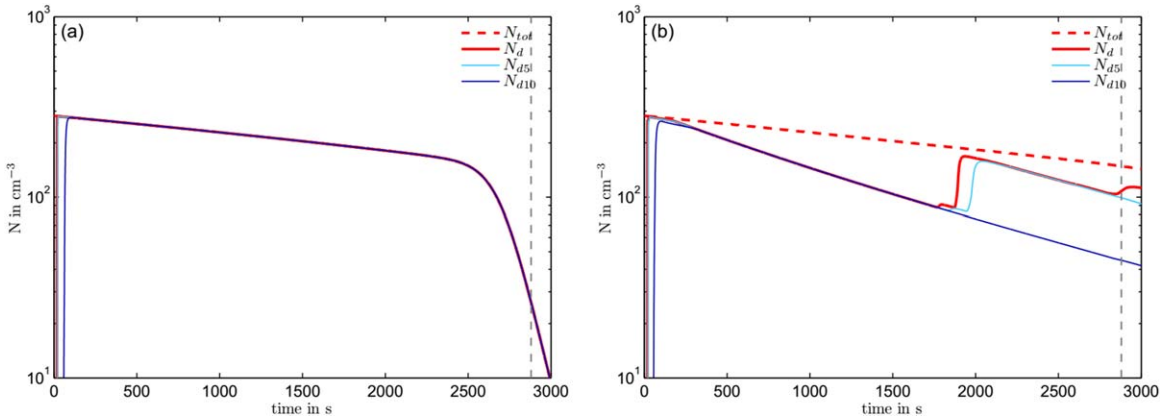

Figure 3. Time evolution of the number concentrations of total particles (unactivated aerosol and droplets; N_{tot}), total droplets (N_d), droplets larger than 5 μm (N_{d5}) and droplets larger than 10 μm in diameter (N_{d10}). Simulations were carried out (a) without entrainment and (b) with entrainment included. Vertical dashed lines indicate the time step analyzed in Figure 4.

Figure 4 shows the simulated distribution of r_{CCN} for one distinct time step (2880 s), the latter being indicated by vertical dashed lines in Figure 3. Left figures show the results without entrainment, and right figures include entrainment. In the first line, r_{CCN} is calculated as a mean value of equal-sized drops for each drop diameter. In line 2, the colors illustrate the frequencies of occurrence of r_{CCN} on a logarithmic scale, each "count" corresponding an individual droplet.

In the top figures, we can clearly distinguish the regimes of condensational growth and collisional growth: As expected, in the condensation regime r_{CCN} decreases with increasing drop size because the aerosol mass within a drop is not affected by condensation. In the collision regime, r_{CCN} is approximately constant when averaged within the drop size bins (Figure 4a)—this is valid throughout the simulation without entrainment. Nevertheless, the stochastic nature of droplet collisions yields a variability of r_{CCN} for a given drop size which comprises about one order of magnitude from minimum to maximum values (Figure 4c).

A more complicated behavior is evident when entrainment is included (Figures 4b and 4d). As described above, an event of in-cloud CCN activation occurs at 1800 s. Prior to this event, $r_{CCN}(D_d)$ is rather flat for droplets larger than 30 μm (not shown). Afterward, raindrops larger than 100 μm tend to have increased values relative to the smaller drops, and the increase tends to continue in time (not shown). Larger r_{CCN} corresponds to the collection of smaller cloud droplets, i.e., the secondary activation event provides the droplets which cause the enhancements of r_{CCN} of larger drops at later times. The drop size-dependent variability of $r_{CCN}(D_d)$ appears to be within a factor of 2 for drops between 30 μm and 3 mm which is still small compared to the variability of r_{CCN} for equally sized drops. Nevertheless, the assumption of constant r_{CCN} during the freezing process would tend to overestimate the freezing rates of small droplets (say, $D < 200$ μm which make the major contribution to the bulk raindrop number concentration), and underestimate the freezing probabilities of larger drops.

The impact of nonconstant $r_{CCN}(D)$ on freezing rates is shown in Figure 4 (bottom). Red lines indicate the freezing rates calculated from a spectrum-averaged r_{CCN} ($D > 80$ μm) corresponding to the bulk model assumption. Black lines result from the consideration of $r_{CCN}(D)$ as shown in Figures 4a and 4b. Even in the simulation with entrainment included (Figure 4f), the spectrum-integrated difference between the freezing rates is smaller than 6%.

In convective clouds, we expect the entrainment effects to be more relevant close to the cloud edges than within the convective core. Based on the SPECS simulations discussed here, this means that the assumption of r_{CCN}=*const*. holds very well within the convective core. In case of CCN activation associated with entrainment, the freezing of small rain-sized drops associated with cloud ice formation tends to be overestimated in the bulk model to a small extent. We conclude that the simple assumptions made for the budgeting and freezing of rain-immersed aerosol particles are appropriate for use in bulk microphysical schemes.

Another conclusion from these simulations concerns the calculation of droplet volume-dependent freezing rates, which implicitly assumes that the aerosol content is proportional to the drop masses [e.g., *Bigg*, 1953].

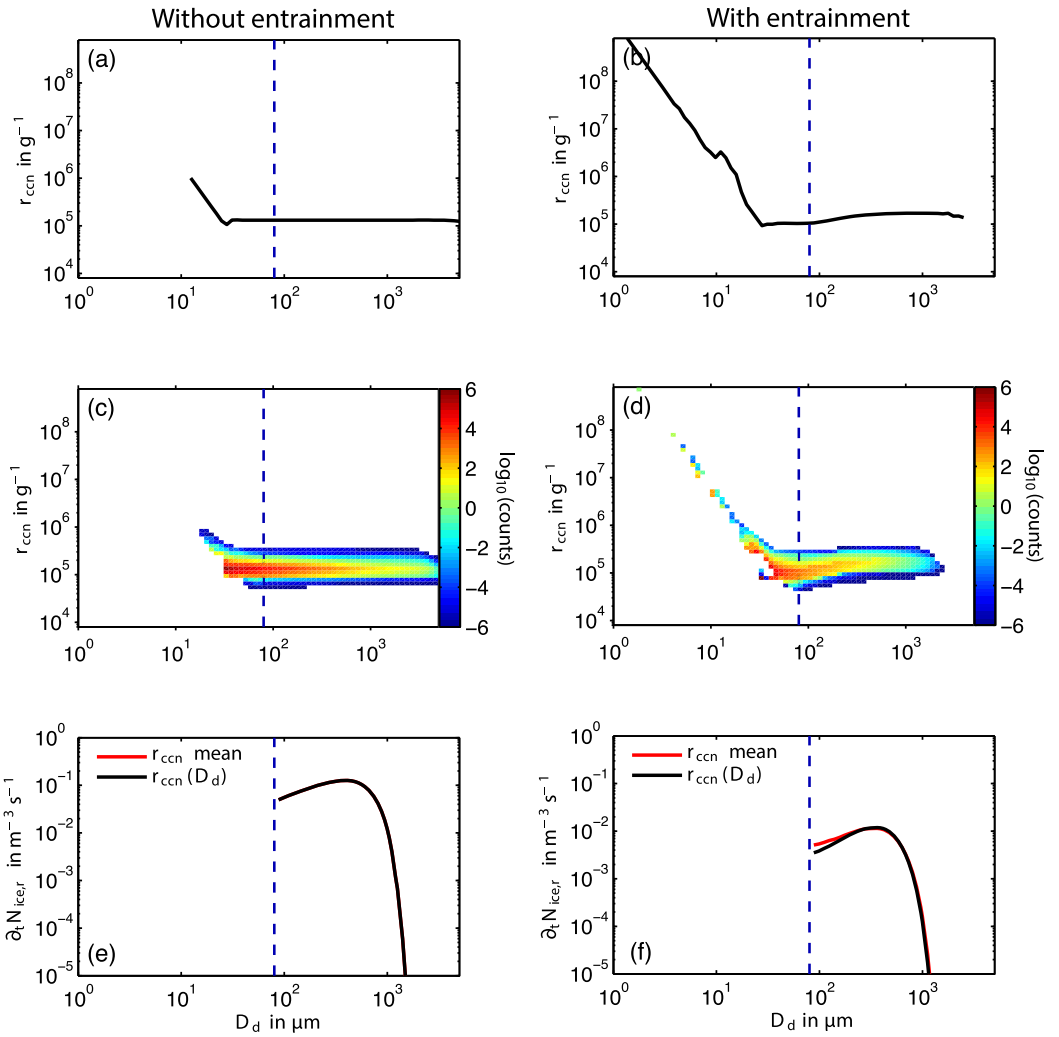

Figure 4. Simulated r_{CCN} and freezing rates (a, c, e) without and (b, d, f) with entrainment shown for a time step in the late stage of the simulation. Top figures illustrate the mean value for equal-sized drops as a function of drop size. Middle figures indicate the variability of r_{CCN} for each drop size, with one "count" of the frequency of occurrence corresponding to a single droplet. Bottom figures show the comparison of freezing rates based on the simulated $r_{CCN}(D_d)$ (black) and based on a mean value representative for the bulk rain properties (red). Vertical dashed lines indicate the separation size between cloud and raindrops at 80 µm.

Our results suggest that the volume-dependent immersion freezing rates is problematic for those droplets which have grown from the vapor phase, since condensation decouples drop mass and aerosol content, the latter being ultimately responsible for heterogeneous droplet freezing.

4. Simulations of Deep Convective Clouds

Here we apply the model implementations to three-dimensional simulations of deep convective clouds. After an introduction to the model setup and simulated clouds, this section will show the collection rates and simulated droplet properties. Afterward, the freezing rates and cloud properties are discussed, comparing the B53 and P17 implementations of drop freezing.

For simplicity, the vertical profiles shown in the following figures are calculated by conditional averaging over areas where $w > 5\,\mathrm{m\,s^{-1}}$, indicated by $<w_5>$ symbols within the figure panels. These profiles are representative for the convective core, while other grid points are excluded from the horizontal mean values. In contrast, precipitation fluxes are calculated as domain averages, indicated by $<*>$ symbols. The data contain the 10 min-spaced model output from 20 to 120 min of the cloud evolution.

4.1. COSMO Model Setup

Our host model is based on the nonhydrostatic limited-area COSMO model [*Baldauf et al*., 2011; *Vogel et al*., 2009], used with a horizontal grid spacing of 500 m, a stretched vertical grid with 100 levels and a time step of 3 s. The extent of the model domain comprises 300 × 250 grid points, and 22 km in the vertical direction. A prognostic three-dimensional turbulence scheme is applied to parameterize subgrid turbulent diffusion of heat, mass and momentum [*Herzog et al*., 2002a, 2002b].

The two-moment bulk microphysics scheme is based on *Seifert and Beheng* [2006] in order to predict mass and number densities of six hydrometeor classes, i.e., cloud and raindrops, cloud ice, snow, graupel, and hail. The particle size distributions are defined by generalized gamma distributions with respect to particle mass x.

Primary ice formation is represented by a number of different mechanisms: In liquid-containing regimes, immersion freezing as described in this paper, and homogeneous freezing [*Cotton and Field*, 2002; *Jeffery and Austin*, 1997] initiate ice. In the cirrus regime, cloud ice can result from deposition nucleation [*Ullrich et al*., 2017] and homogeneous freezing of solution droplets [*Kärcher et al*., 2006].

In sets of three different simulations, we specify dust number concentrations of $N_{dust} = 10^4\ \mathrm{m}^{-3}$, $10^5\ \mathrm{m}^{-3}$, and $10^6\ \mathrm{m}^{-3}$ in the lower atmosphere. This only affects ice nucleation, while CCN activation following *Segal and Khain* [2006] is independent of mineral dust. The concentration of boundary layer condensation nuclei is defined as $1.7 \times 10^9 \mathrm{m}^{-3}$, representative for continental aerosol environments.

We rely on a well-known and widely used [e.g., *Morrison and Milbrandt*, 2011] idealized test case, originally introduced by *Weisman and Klemp* [1982] to investigate the dynamics of isolated thunderstorms in different environments with respect to vertical wind shear and boundary layer humidity. For this study we choose a low-level water vapor mixing ratio of $14\ \mathrm{g\,kg}^{-1}$ and a vertical wind shear of $25\ \mathrm{m\,s}^{-1}$ which results in a supercell type of convection. Following *Weisman and Klemp* [1982], the wind shear is unidirectional, yielding a quasi-symmetric cloud evolution after the initial cell splitting. The example of precipitation sensitivity (section 4.5) is based on a weaker type of convective cell, with $10\ \mathrm{m\,s}^{-1}$ vertical wind shear and a boundary layer humidity of $11\ \mathrm{g\,kg}^{-1}$.

As the simulations with each three dust concentrations are conducted with both the B53 and the P17 schemes for drop freezing, this results in six simulations, which are analyzed in the following. In addition, sensitivity experiments with respect to individual microphysical processes are based on the case with P17 and $N_{dust} = 10^5\ \mathrm{m}^{-3}$.

4.2. Redistribution of Mineral Dust

Figure 5a shows the rates of cloud selfcollection, cloud autoconversion, and accretion by rain which result in the conversion of cloud droplet-immersed CCN to rain droplet-immersed CCN. Accretion makes the

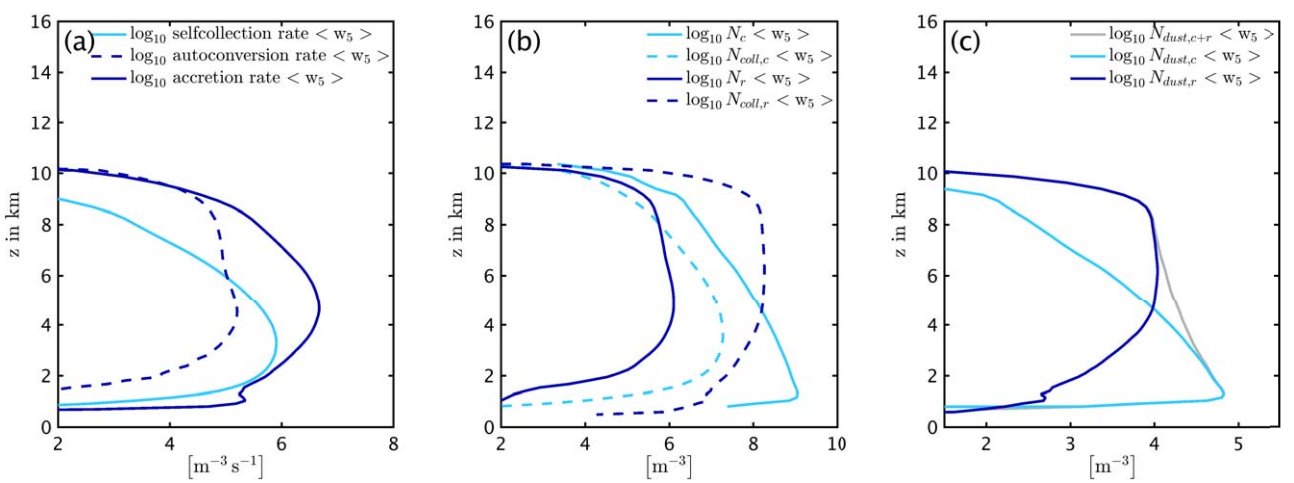

Figure 5. (a) Collision rates of cloud and raindrops, (b) number concentrations of cloud droplets, raindrops and collected particles, and (c) number concentrations of cloud-immersed dust, rain-immersed dust and the sum of both. Shown are the vertical profiles averaged over updraft regimes $<w_5>$. Note that the *x* axes are labeled with the decadal logarithms of the variables in the indicated units.

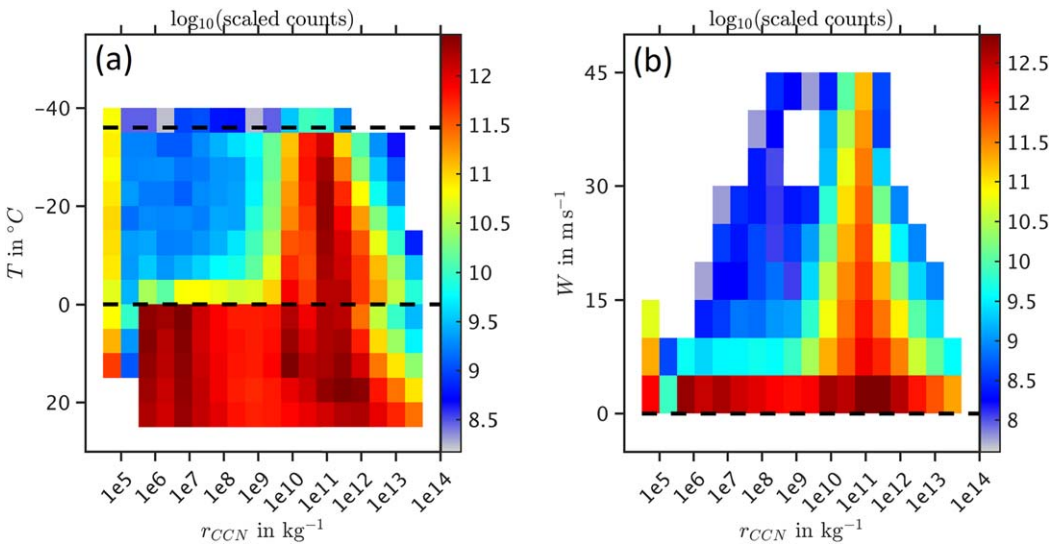

Figure 6. Joint histograms of collected CCN per rain mass (r_{CCN}) shown as a function of (a) temperature and (b) vertical velocity. The counts are scaled by grid box volume such that each cubic meter of air in the model corresponds to one count in the plotted data. Horizontal dashed lines in Figure 6a indicate the levels of 0 °C and −36 °C.

highest contribution in all levels, with a maximum from 4 to 5 km corresponding to slight supercooling. The peak of the selfcollection contribution is below 4 km, where N_c is larger than above. Although the mean rate is around $10^6\,\mathrm{m}^{-3}\,\mathrm{s}^{-1}$, it is rather small compared to the high number of cloud droplets. The autoconversion contribution to the accumulation of CCN in rain is very small compared to accretion.

The concentrations of collected CCN in cloud and raindrops are indicated by dashed lines in Figure 5b. In the convective core region, $N_{coll,r}$ is on average at least two orders of magnitude larger than N_r, i.e., raindrops contain on average more than 100 particles. This is different for cloud droplets which contain on average less than one collected CCN. Note that according to section 2.1, $N_{coll,c}$ does not contain those CCN which activated the droplet at cloud base, therefore it can be smaller than N_c. The resulting mineral dust concentrations immersed in cloud and raindrops are shown in Figure 5c, according to equation (14).

As expected, potential IN particles are slowly shifted from cloud to raindrops during ascent. They are equally distributed ($N_{dust,c} \approx N_{dust,r}$) around the melting level, but in general, this will depend on several cloud properties like cloud base height, conversion efficiency and therefore the initial cloud droplet number, and updraft speed. At altitudes of the highest mineral dust immersion freezing activities, $N_{dust,c}$ is 1 to 2 orders of magnitude smaller than $N_{dust,r}$.

A more detailed analysis is presented in the joint histograms in Figure 6 which shows the r_{CCN} frequencies of occurrence based on the simulated properties of rain. In Figure 6a, r_{CCN} as a function of temperature shows a high variability of several orders of magnitude. The smaller values ($r_{CCN} < 10^9\ \mathrm{kg}^{-1}$) below the melting level arise from the neglected tracking of aerosols in ice-phase hydrometeors, and thus the lack of aerosols in rains drops which are generated by melting. The areas of rain formation by melting are widespread compared to the convective core and result therefore in large numbers of counts of small r_{CCN}. Figure 6b displays r_{CCN} as a function of updraft velocity w. Accordingly, the most pronounced accumulation of CCN (highest values of r_{CCN}) appears in updrafts with $w < 5\,\mathrm{m\,s}^{-1}$, i.e., when the drops are balanced within an updraft for a longer time in a quasi steady state. In stronger updrafts, a relatively narrow distribution of r_{CCN} is found around 10^{11} particles per kg of rainwater. This corresponds to a mean diameter of collected cloud droplets around 25–30 μm. Drops with diameters of 100 and 500 μm would thus contain around 50 and 7000 CCN, respectively.

4.3. Freezing Rates

Here we begin without the consideration of PSD splitting, treating the rain spectrum as a whole (see section 2.3). The effect of PSD splitting and further sensitivity studies is shown below in this section. At this

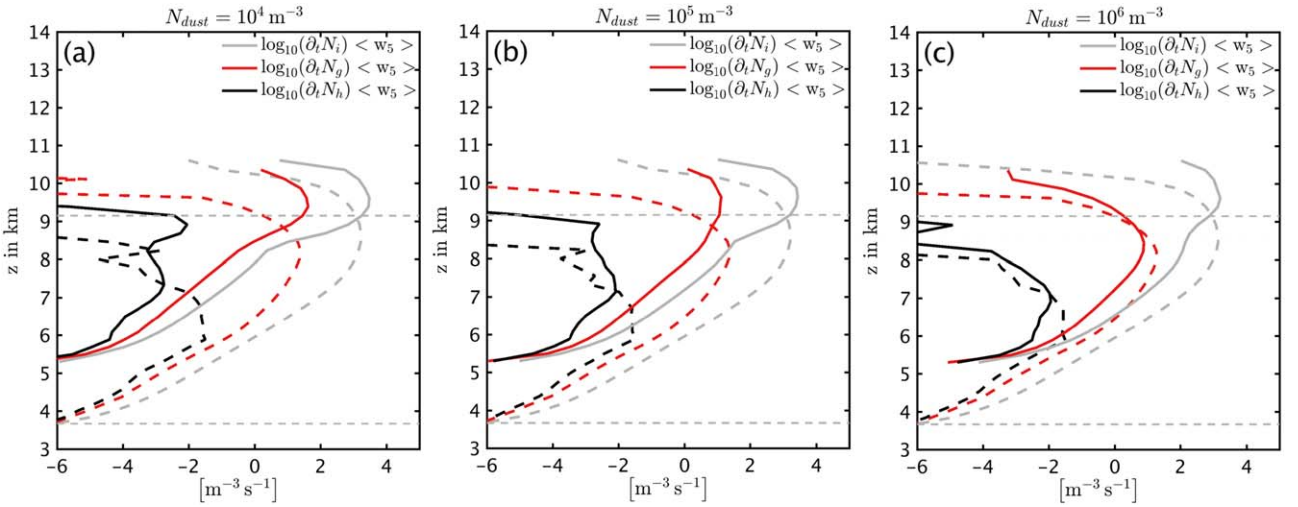

Figure 7. Formation rates of cloud ice, graupel, and hail by freezing rain with (a) $N_{dust}=10^4\ \mathrm{m}^{-3}$, (b) $N_{dust}=10^5\ \mathrm{m}^{-3}$, and (c) $N_{dust}=10^6\ \mathrm{m}^{-3}$. Dashed lines result from B53, and full lines from the new P17 implementation. Horizontal dashed lines indicate the levels of 0 °C and −36 °C. Note that the *x* axes are labeled with the decadal logarithms of the variables in the indicated units.

point, we note that the primary effect is found for the formation rates of hail particles which is modified by a factor of 2.

Figure 7 compares the freezing rates of rain in the convective updraft, based on the IN-dependent parameterization (this study, full lines) and the B53-based default parameterization (dashed lines). Figures 7a–7c are the results for different ice nuclei concentrations, with N_{dust} ranging from 10^4 to $10^6\ \mathrm{m}^{-3}$.

According to the model implementation [*Seifert and Beheng*, 2006, equation (44)], the B53-based freezing starts to form ice at 0 °C, while ice nucleation on mineral dust particles (N12) is parameterized only for temperatures lower than −12 °C. With more dust, ice formation rates predicted by P17 become more similar to the B53 approach, but are smaller even with $10^6\ \mathrm{m}^{-3}$ dust particles. The magnitude of the homogeneous freezing peak is nearly independent of the dust concentration, indicating that even with the highest concentration the number of small drops cannot be reduced significantly by heterogeneous freezing. A higher dependence of upper level freezing rates on the immersion freezing efficiency is found for graupel and hail formation. With less dust, more ice is formed in upper levels because of a less efficient depletion of large raindrops. Except for the lowest dust concentrations (a), hail is most efficiently formed in the heterogeneous freezing region.

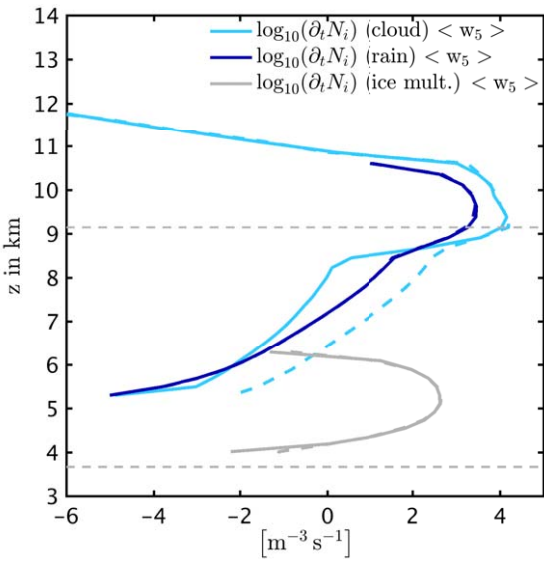

Figure 8. Freezing rates of cloud droplets, raindrops, and secondary ice formation rates, shown as a comparison between reduced cloud-immersed dust (full lines) and with all dust particles attributed to cloud droplets (dashed lines). Both simulations include the P17 immersion freezing scheme with $N_{dust}=10^5\ \mathrm{m}^{-3}$. Horizontal dashed lines indicate the levels of 0 °C and −36 °C. Note that the *x* axes are labeled with the decadal logarithms of the variables in the indicated units.

Figure 8 compares the difference between cloud droplet freezing rates with and without accounting for the redistribution of IN from cloud to raindrops. Consistent with Figure 5c, the heterogeneous cloud droplet freezing rates are reduced by roughly 2 orders of magnitude compared to the assumption of all dust being immersed in cloud droplets (dashed light blue line). At the warmest freezing temperatures around −12 °C, cloud and raindrops contribute equally to small ice formation, but rain becomes

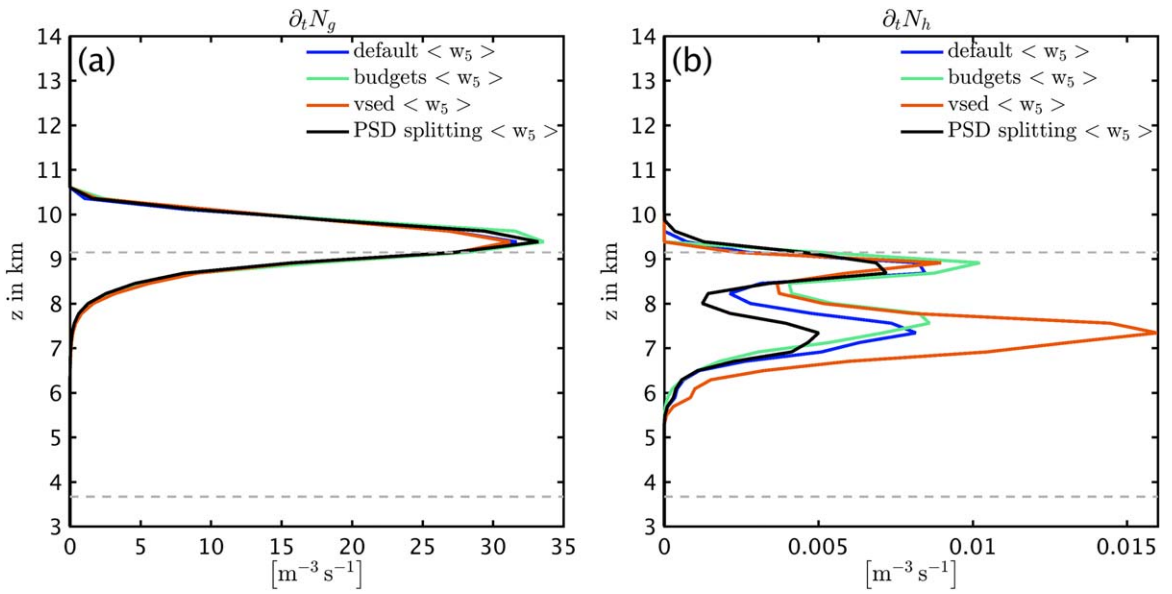

Figure 9. (a) Graupel and (b) hail formation rates by freezing rain, shown for the default version, simplified budgeting ("budgets"), neglected sedimentation velocities ("vsed"), and additional PSD splitting. The "default" corresponds to the simulation with P17 and $N_{dust}=10^5$ m^{-3}, as presented above in this section. Horizontal dashed lines indicate the levels of 0 °C and −36 °C.

more important in upper levels (dark blue). Only above 8 km, the cloud droplet contribution becomes larger than the rain contribution because in the homogeneous freezing regime, the drop number concentration dominates. For comparison, also the production of secondary ice according to *Hallett and Mossop* [1974] at levels around 5 km is shown for comparison. This dominant peak is also reflected in the cloud ice concentrations (see Figure 10 and section 4.4).

Based on this version of the freezing parameterization, further simulations have been conducted to estimate the sensitivity to (a) a simplified budgeting with $N_{coll,c}=0$, no sinks and no sedimentation for $N_{coll,r}$ (see also 4.2), (b) the disregard of the sedimentation velocity during the freezing process (equation (20)), and (c) rain PSD splitting for the freezing parameterization (equations (23)–(27)).

Figure 9 illustrates the sensitivities of graupel and hail formation rates, while cloud ice rates are hardly affected by the different treatments (not shown). Hail formation—which involves the largest drops—is generally most sensitive to the different versions. The "default" version (blue line) shows the profiles which have been analyzed above in this section. The simplified budgeting of $N_{coll,c/r}$ makes only minor differences (green line). However, accounting for the drop sedimentation of large drops appears to be important: With $v_{sed}=0$ by definition, the cooling rates of large drops are overestimated, and therefore hail formation in mid levels (Figure 9b, orange line) is twice as large as the reference. By including PSD splitting, the rates are smallest (black): on one hand, for a given dust concentration, multiple IN per drop reduce the number of freezing drops. On the other hand, with PSD splitting the effect of smaller cooling rates of larger drops becomes more pronounced. Note that the simulations shown here are based on $N_{dust}=10^5$ m^{-3}, while the effect of multiple IN per drop will be more pronounced with higher concentrations.

4.4. Ice Particle Concentrations and Sedimentation Fluxes

An overview of the differences in the number concentrations of small ice, graupel, and hail is shown in Figure 10. The presence of cloud ice at temperatures warmer than −12 °C, and the local maximum around 5 km in particular, is mainly attributed to ice multiplication by rime splintering (see also Figure 8a). This maximum is not very sensitive to the changes introduced by the different immersion freezing treatments, therefore the cloud ice concentration reduction in the immersion freezing regime is not as pronounced as might be expected from the immersion freezing rates when comparing B53 and P17 (Figures 7 and 8). Graupel behaves as expected from Figure 7, with less particles below 9 km and more particles above the homogeneous freezing level when using P17 (i.e., dust-based freezing). Hail numbers are reduced throughout the updraft, i.e., the larger formation rates at $z>8$ km cannot compensate for the smaller rates below (Figure 7).

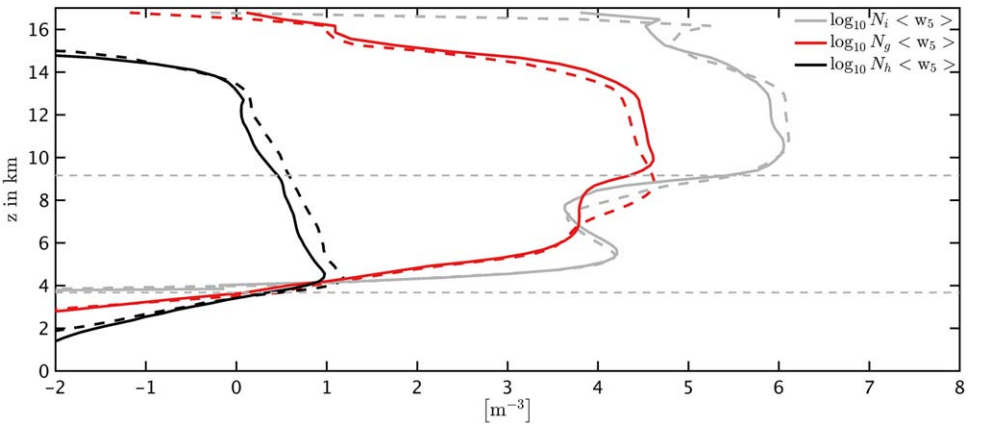

Figure 10. Number concentrations of cloud ice, graupel, and hail as a comparison of B53 (dashed lines) and P17 immersion freezing (full lines), with $N_{dust} = 10^5$ m^{-3}. Horizontal dashed lines indicate the levels of 0 °C and −36 °C. Note that the *x* axes are labeled with the decadal logarithms of the variables in the indicated units.

Although the number changes do not appear to be dramatic, they have important implications for the growth of large precipitating particles by riming and subsequent sedimentation properties. Figure 11 shows domain-averaged sedimentation fluxes. The "effective" fluxes of rain ($R_\downarrow$), graupel ($G_\downarrow$), and hail ($H_\downarrow$) account only for those regions in which mass effectively sediments, while considering the vertical advection. Therefore, the flux of particle class *x* is calculated as $(v_{qx} - w)\, Q_x$, with v_{qx} being the sedimentation velocity of the first moment of *x* (positive downward).

The rain flux (blue) can be divided into two distinct regimes, that is, the area below 4 km corresponding to the melting regime and rain at the edges of the convective core in regions of small positive and negative vertical velocities. At z > 4 km, it is evident that the P17 freezing leaves behind more rain mass (full line). Particularly in the sedimenting regime, this is also a result of the v_{sed}-dependent freezing rates.

Generally, graupel and hail flux changes have opposite signs when the immersion freezing efficiency is modified. With smaller immersion freezing rates (P17), the hail flux is significantly larger although it was shown that the hail number is smaller throughout the updraft, implying larger mean particle masses. With the higher upper level graupel number density and a lower mass density (not shown), graupel sedimentation efficiency is decreased. Snow hardly contributes to melting because in the sedimentation regimes outside of the convective core, the slowly falling particles sublimate in upper levels, and the same applies for cloud ice. The largest relative flux changes are found for hail which is up to more than a factor of 5 larger near ground with P17. However, these differences can be strongly time-dependent with a tendency of decreased relative differences at later times (not shown).

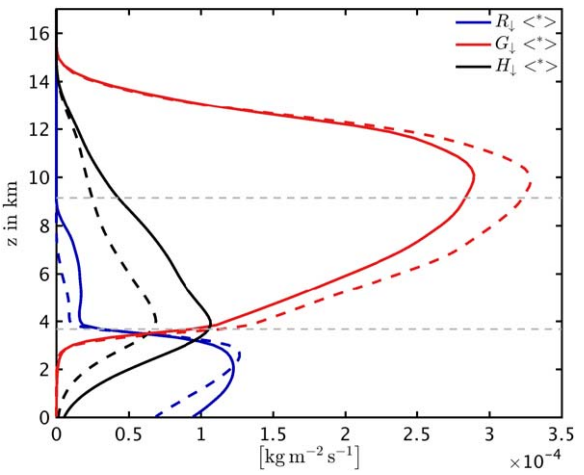

Figure 11. Effective sedimentation fluxes of graupel, hail, and rain as a comparison of B53 (dashed lines) and P17 immersion freezing (full lines), with $N_{dust} = 10^5$ m^{-3}.

4.5. Sensitivities of Precipitation to Ice Nuclei Perturbations

Finally, we highlight the relevance of aerosol-dependent rain freezing for simulations of precipitation sensitivities to IN. Figure 12 shows a comparison between the implementations, B53 and P17. Δ indicates the difference between two simulations with different aerosol state, i.e., "more minus less IN." Different from the supercell simulation discussed above, here we analyze a weaker type of cell which is about to dissipate after about 1 h (see section 4.1). In this case, the hail contribution to the surface rain formation is less

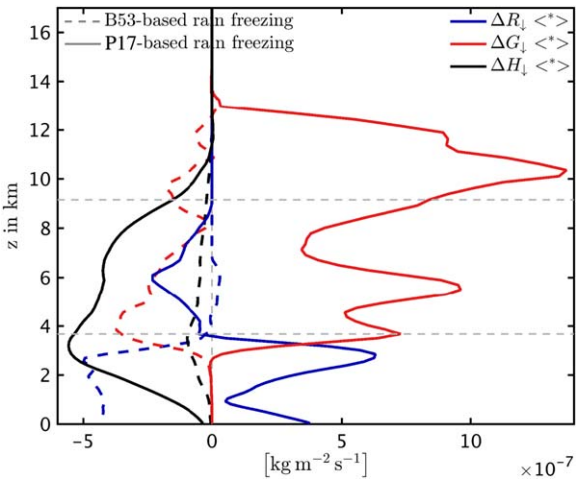

Figure 12. Precipitation sensitivity to IN perturbations as a comparison of B53 (dashed lines) and P17 immersion freezing (full lines), with Δ indicating the difference between two simulations of $N_{dust} = 10^6\ \mathrm{m}^{-3}$ and $N_{dust} = 10^5\ \mathrm{m}^{-3}$, respectively. Horizontal dashed lines indicate the levels of $0\ ^\circ\mathrm{C}$ and $-36\ ^\circ\mathrm{C}$.

pronounced, thus emphasizing the importance of simulated graupel properties and resulting in a stronger sensitivity to IN then in the supercell case.

Several differences are evident from Figure 12. The depletion of supercooled rain mass ($z > 4$ km) is more pronounced with explicit IN dependence of rain freezing. In both cases, B53 and P17, hail precipitation is reduced with more IN present. With dust-based freezing, the reduction of hail is more pronounced, given the importance of riming and the presence of supercooled rain mass. Most importantly, the sensitivity of graupel precipitation has an opposite sign when simulated with explicit aerosol dependence. Since the surface rain flux is dominated by the melting of graupel below 4 km in this example of weaker convection, also the change of surface rain has an opposite sign.

The attribution of this behavior to specific mechanisms will be the subject of a follow-up study. However directly related to the treatment of freezing, an important feature may be the less efficient B53-based rain freezing with more IN present: the increased amount of IN within cloud droplets results in an increased amount of cloud ice. Via the pathway of riming, also rain mass is removed more efficiently. With the sole dependence on rain mass (equation (1)), rain freezing is less efficient with more IN present, thus creating less graupel by freezing. This is different from the results with explicit IN dependence, where more IN yield more graupel by freezing, and a more efficient growth of the bulk of graupel.

5. Summary and Discussion

In this paper we presented a novel approach of parameterizing the aerosol-dependent freezing of large drops (rain/drizzle drops) in bulk microphysical models. The framework consists of two parts, that is, (a) the tracking of drop microphysical histories and therefore case-specific particle accumulation and (b) a freezing parameterization to consider multiple ice nuclei (IN) per drop and effective drop cooling rates. The assumption of homogeneously distributed particles among the rain mass was validated using a two-dimensional bin microphysical model.

In our test cases of deep convective cells, it was found that in the regimes most relevant for immersion freezing, the majority of potential IN is contained in raindrops. This also implies that the freezing probabilities of cloud droplets are rather insensitive to IN perturbations, as most of them freeze homogeneously. In other types of clouds—e.g., with colder cloud bases or thinner, stratiform clouds without significant collision-coalescence—more emphasis may be put on cloud droplets. The consideration of multiple IN per drop as well as drop sedimentation is particularly important for the subset of largest drops, affecting the formation of hail embryos.

To optimize computational efficiency, it would be desirable not to track collision rates by making use of additional model tracers. While the consideration of cloud droplet selfcollection—i.e., multiple cloud droplet-immersed CCN—had only a minor impact in our simulations, particle accumulation in rain is not negligible. Since it is likely that the effect of redistribution is highly dependent on the particular cloud properties, such as initial droplet number, updraft velocity and cloud depth, it may be worth developing simple parameterizations of r_{CCN} for further use in freezing schemes. To our knowledge, no methods exist for this purpose to date. Cloud resolving simulations of a variety of different cloud regimes would be needed to derive simple relationships between r_{CCN} and commonly predicted cloud properties.

We compared the freezing rates and cloud properties which result from the IN-independent approach following B53 and the mineral dust-based immersion freezing according to the dust properties of N12 with the above-described tracking of dust in cloud droplets and raindrops (P17). With cloud-base mineral dust concentrations ranging from $10^4\,m^{-3}$ to $10^6\,m^{-3}$, the dust-based freezing rates (P17) are generally smaller than B53-based rates. This has important implications for the relative importances of homogeneous and heterogeneous freezing: While the efficient B53-based drop freezing depletes the majority of liquid mass below the homogeneous freezing regime, many drizzle-sized drops ($D > 80$ μm) can reach these levels when heterogeneous freezing is triggered by dust only. This seems reasonable when raindrops are more numerous than a limited concentration of dust particles. With the small efficiency of drop depletion by freezing, we speculate whether in strong convection it may be common to find large drops at temperatures below −30 °C, or whether we miss important mechanisms in the model, such as additional types of IN like organic particles [*Knopf et al*., 2014]. If we consider large drops in such regimes rather unlikely, we may conclude that mineral dust cannot be the dominant particle species for immersion freezing in the coldest portion of the mixed-phase regime—assuming that the microphysical interactions other than freezing are represented appropriately in the model.

The number of rain-sized drops which are able to reach the homogeneous freezing regime also depends on factors other than IN concentrations: The efficiency of raindrop formation is determined by the initial cloud droplet size distribution and therefore CCN concentrations, and the time to reach the colder levels results from both cloud-base temperature (i.e., altitude) and convective strength. Although more time is available for raindrops to form in slower updrafts, the chance of drop depletion by riming increases, thus promoting the glaciation of the mixed-phase regime. The clouds simulated in this work represent very strong supercell convective clouds with relatively warm cloud bases. Thus, the microphysical behavior of weaker convective clouds should be the subject of future efforts in order to enable a validation of modeled upper level liquid water content with available measurements, which may help to constrain the role of upper level immersion freezing of mineral dust and other aerosol particles.

Rosenfeld and Woodley [2000] observed high liquid water contents in deep convective clouds down to −37.5 °C, although the majority of droplets was smaller than 20 μm in diameter. This situation was reproduced successfully in the model simulations of *Khain et al*. [2001], suggesting three conditions to find high amounts of supercooled liquid water: high concentrations of CCN yield numerous but small cloud droplets, making the conversion to rain inefficient, and the efficiencies of droplet freezing small. Furthermore, the formation of relatively small graupel resulted in inefficient riming, promoting a dominant homogeneous droplet freezing in upper levels. In contrast, a more efficient glaciation was found with maritime CCN concentrations, yielding rain-sized drops by collision-coalescence, higher freezing probabilities, and larger graupel particles supported the faster glaciation by riming. Furthermore, *Khain et al*. [2001] note that the consideration of turbulence may influence the simulated riming rates significantly. They conclude that often models are unable to reproduce the persistence of highly supercooled liquid because of overestimated rates of raindrop formation and associated high freezing probabilities of large drops. In our implementation, whether or not the formation of rain-sized drops is overestimated may be of secondary importance in terms of freezing efficiency: although freezing still depends on the autoconversion efficiency and drop sizes, the main factor to determine the freezing probability is given by the fraction of mineral dust particles compared to the CCN at cloud base.

Based on our comparison of dust-dependent freezing and the more efficient ice formation according to *Bigg* [1953], it is also unclear whether the widely used standard approach for droplet freezing in models tends to overestimate cloud glaciation considerably under average atmospheric conditions. Here we suggest that—aside from any aerosol dependencies—the parameterized freezing rates of raindrops should not be completely independent of the drop effective cooling rate. Otherwise, even continuously warming drops are allowed to freeze. Consistent with the singular hypothesis [*Vali and Stansbury*, 1966; *Vali*, 1994], none of the droplets falling from colder into warmer regions may freeze by immersion freezing in our scheme. Obviously, the specific model formulation and underlying assumptions add considerable room for uncertainty, in addition to the uncertainties caused by aerosol properties.

In the simulations of deep convective clouds, our implementation has major effects on the supercooled liquid water content, and thus on precipitation formation. With more liquid present in the mixed-phase regime of the convective core, the largest relative differences are observed in the simulated hail

precipitation flux, owing to the growth mechanism of riming. We also show that in particular for graupel precipitation, the simulated sensitivity to changes in the IN concentration has opposite signs when comparing the B53 and P17 freezing schemes. This difference is particularly important in weak convective clouds when graupel dominates the formation of surface rain.

Based on the freezing scheme presented in here, a detailed sensitivity analysis of precipitation and radiation to ice nuclei perturbations will be the subject of a follow-up publication. Future work should aim at constraining drop freezing efficiencies by using observations of convective clouds. This may become feasible as multi-radar observations become increasingly popular to infer cloud particle size distributions [*Kneifel et al.*, 2016; *Tridon and Battaglia*, 2015].

Notation

a	parameter according to *Bigg* [1953], K^{-1}.
a_{N12}	parameter according to *Niemand et al.* [2012], K^{-1}.
A	coefficient of the generalized Gamma-distribution, $kg^{-(\nu+1)}m^{-3}$.
b	parameter according to *Bigg* [1953], $m^{-3}\,s^{-1}$.
b_{N12}	parameter according to *Niemand et al.* [2012], 1.
B	exponent of the generalized Gamma-distribution, $kg^{-\mu}$.
$dN_{c,au}$	autoconversion rate of cloud droplets, $m^{-3}\,s^{-1}$.
$dN_{c,acc}$	accretion rate of cloud droplets by rain, $m^{-3}\,s^{-1}$.
$dN_{c,sc}$	selfcollection rate of cloud droplets, $m^{-3}\,s^{-1}$.
D	diameter of aerosol particles and hydrometeor species, m.
$f(x)$	number density function with respect to particle mass, $m^{-3}\,kg^{-1}$.
$f_{dust,cb}$	cloud-base fraction of mineral dust relative to total CCN, 1.
$G_{\downarrow}$	downward effective mass flux of graupel, corrected for vertical advection, $kg\,m^{-2}\,s^{-1}$.
γ	lower incomplete gamma function, 1.
Γ	complete gamma function, 1 .
$H_{\downarrow}$	downward effective mass flux of hail, corrected for vertical advection, $kg\,m^{-2}\,s^{-1}$.
k	coefficient of the probability mass function, 1.
λ_c	mean number of collected CCN per cloud droplet, 1.
λ_{IN}	mean number of activated IN per raindrop, 1.
μ	exponent of the generalized Gamma-distribution, 1.
$n_s(T_c)$	ice nucleation active surface site density, m^{-2}.
$n_{dust,r}(D)$	lognormal size distribution of dust particles immersed in raindrops, m^{-4}.
n_r	number density of raindrops in a finite interval of $f(x)$, m^{-3}.
N_{CCN}	number density of CCN, m^{-3}.
$N_{coll,c/r}$	number density of collected CCN in cloud and rain droplets, m^{-3}.
N_d	SPECS-simulated number density of droplets, m^{-3}.
N_{d5}	SPECS-simulated number density of droplets larger than 5 μm, m^{-3}.
N_{d10}	SPECS-simulated number density of droplets larger than 10 μm, m^{-3}.
N_{dust},	number density of mineral dust in the lower atmosphere, m^{-3}.
$N_{dust,c/r}$	dust particles available as potential IN within cloud/rain droplets, m^{-3}.
$N_{ice,r}$	number density of ice particles (i, g, h) formed by freezing rain, m^{-3}.
$N_{IN,r}$	number density of activated IN in the bulk mass of rain, m^{-3}.
N_{tot},	SPECS-simulated number density of aerosols and droplets, m^{-3}.
N_x,	number density of particle class $x \in \{c, r, i, s, g, h\}$, m^{-3}.
ν	exponent of the generalized Gamma-distribution, 1.
$P(X)$	probability mass function of a discrete random variable X, 1.
q_r	mass density of raindrops in a finite interval of $f(x)$, $kg\,m^{-3}$.
Q_x	mass density of particle class $x \in \{c, r, i, s, g, h\}$, $kg\,m^{-3}$.
r_{CCN}	CCN number concentration per droplet liquid mass, kg^{-1}.
$R_{\downarrow}$	downward effective mass flux of rain, corrected for vertical advection, $kg\,m^{-2}\,s^{-1}$.
ρ_w	density of liquid water, $kg\,m^{-3}$.
$S_{dust,r}$	total surface area of rain-immersed dust particles per volume of air, $m^2\,m^{-3}$.

$\bar{S}_{dust,r}$	mean surface area of rain-immersed dust particles, m^2.
T	temperature, K .
T_c	temperature, °C .
v_{qx}	sedimentation velocity of the first moment of particle class x (positive downward), $m\,s^{-1}$.
v_{sed}	single particle sedimentation velocity (positive downward), $m\,s^{-1}$.
w	vertical velocity, $m\,s^{-1}$.
x	cloud particle mass, kg .
x_{80}	mass of a drop with $D=$ 80 μm, kg.
$x_{coll,r}$	mean raindrop mass per immersed CCN, kg.
x_{ubd}	upper boundary at mass x for partial integration of $f(x)$, kg.
z	vertical coordinate, m.

Acknowledgments
The authors would like to thank Axel Seifert for helpful discussions, and Bernhard Vogel and Max Bangert for providing the model basis used in this study. Primary data analyzed in this study are available from the authors upon request. This research was funded by the Helmholtz Association through the Climate Initiative REKLIM and the President's Initiative and Networking Fund (VH-NG-620) and by the DFG through FOR 1525 INUIT (HO 4612/1-1 and HO 4612/1-2).

References

Baldauf, M., A. Seifert, J. Förstner, D. Majewski, M. Raschendorfer, and T. Reinhardt (2011), Operational convective-scale numerical weather prediction with the COSMO model: Description and sensitivities, *Mon. Weather Rev.*, *139*(12), 3887–3905, doi:10.1175/MWR-D-10-05013.1.

Barklie, R. H. D., and N. R. Gokhale (1959), The freezing of supercooled water drops, *Sci. Rep. MW-30*, pp. 43–64, Stormy Weather Group, McGill Univ., Montreal, Que., Canada.

Bauer, P., A. Thorpe, and G. Brunet (2015), The quiet revolution of numerical weather prediction, *Nature*, *525*(7567), 47–55, doi:10.1038/nature14956.

Beheng, K. D., and F. Herbert (1986), Mathematical studies on the aerosol concentration in drops changing due to particle scavenging and redistribution by coagulation, *Meteorol. Atmos. Phys.*, *35*(4), 212–219, doi:10.1007/BF01041813.

Bigg, E. K. (1953), The formation of atmospheric ice crystals by the freezing of droplets, *Q. J. R. Meteorol. Soc.*, *79*(342), 510–519, doi:10.1002/qj.49707934207.

Blahak, U. (2008), Towards a better representation of high density ice particles in a state-of-the-art two-moment bulk microphysical scheme, paper presented at 15th International Conference on Clouds and Precipitation, Cancun, Mexico.

Boucher, O., et al. (2013), Clouds and aerosols, in *Climate Change 2013: The Physical Science Basis. Contribution of Working Group I to the Fifth Assessment Report of the Intergovernmental Panel on Climate Change*, edited by T. F. Stocker et al., Cambridge Univ. Press, Cambridge, U. K.

Braham, R. R. (1964), What is the role of ice in summer rain-showers?, *J. Atmos. Sci.*, *21*(6), 640–645, doi:10.1175/1520-0469(1964)021 < 0640:WITROI>2.0.CO;2.

Cotton, R. J., and P. R. Field (2002), Ice nucleation characteristics of an isolated wave cloud, *Q. J. R. Meteorol. Soc.*, *128*(585), 2417–2437, doi:10.1256/qj.01.150.

Diehl, K., and S. K. Mitra (2015), New particle-dependent parameterizations of heterogeneous freezing processes: Sensitivity studies of convective clouds with an air parcel model, *Atmos. Chem. Phys.*, *15*(22), 12,741–12,763, doi:10.5194/acp-15-12741-2015.

Garrett, T. J., L. Avey, P. I. Palmer, A. Stohl, J. A. Neuman, C. A. Brock, T. B. Ryerson, and J. S. Holloway (2006), Quantifying wet scavenging processes in aircraft observations of nitric acid and cloud condensation nuclei, *J. Geophys. Res.*, *111*, D23S51, doi:10.1029/2006JD007416.

Hallett, J., and S. C. Mossop (1974), Production of secondary ice particles during the riming process, *Nature*, *249*, 26–28.

Hartmann, S., S. Augustin, T. Clauss, H. Wex, T. Šantl Temkiv, J. Voigtländer, D. Niedermeier, and F. Stratmann (2013), Immersion freezing of ice nucleation active protein complexes, *Atmos. Chem. Phys.*, *13*(11), 5751–5766, doi:10.5194/acp-13-5751-2013.

Herzog, H.-J., U. Schubert, G. Vogel, A. Fiedler, and R. Kirchner (2002a), LLM—The high-resolving nonhydrostatic simulation model in the DWD-project LITFASS Part I: Modeling technique and simulation method, *Tech. Rep. 4*, Consortium for Small-Scale Modell., Offenbach am Main, Germany.

Herzog, H.-J., G. Vogel, and U. Schubert (2002b), LLM—A nonhydrostatic model applied to high-resolving simulations of turbulent fluxes over heterogeneous terrain, *Theor. Appl. Climatol.*, *73*(1–2), 67–86, doi:10.1007/s00704-002-0694-4.

Hiron, T., and A. I. Flossmann (2015), A study of the role of the parameterization of heterogeneous ice nucleation for the modeling of microphysics and precipitation of a convective cloud, *J. Atmos. Sci.*, *72*(9), 3322–3339, doi:10.1175/JAS-D-15-0026.1.

Hoose, C., and O. Möhler (2012), Heterogeneous ice nucleation on atmospheric aerosols: A review of results from laboratory experiments, *Atmos. Chem. Phys.*, *12*(20), 9817–9854, doi:10.5194/acp-12-9817-2012.

Jeffery, C. A., and P. H. Austin (1997), Homogeneous nucleation of supercooled water: Results from a new equation of state, *J. Geophys. Res.*, *102*(D21), 25,269–25,279, doi:10.1029/97JD02243.

Johnson, J. S., Z. Cui, L. A. Lee, J. P. Gosling, A. M. Blyth, and K. S. Carslaw (2015), Evaluating uncertainty in convective cloud microphysics using statistical emulation, *J. Adv. Model. Earth Syst.*, *7*(1), 162–187, doi:10.1002/2014MS000383.

Kärcher, B., J. Hendricks, and U. Lohmann (2006), Physically based parameterization of cirrus cloud formation for use in global atmospheric models, *J. Geophys. Res.*, *111*, D01205, doi:10.1029/2005JD006219.

Khain, A., M. Ovtchinnikov, M. Pinsky, A. Pokrovsky, and H. Krugliak (2000), Notes on the state-of-the-art numerical modeling of cloud microphysics, *Atmos. Res.*, *55*(3–4), 159–224, doi:10.1016/S0169-8095(00)00064-8.

Khain, A. P., D. Rosenfeld, and A. Pokrovsky (2001), Simulating convective clouds with sustained supercooled liquid water down to −37.5°C using a spectral microphysics model, *Geophys. Res. Lett.*, *28*(20), 3887–3890, doi:10.1029/2000GL012662.

Khain, A. P., et al. (2015), Representation of microphysical processes in cloud-resolving models: Spectral (bin) microphysics versus bulk parameterization, *Rev. Geophys.*, *53*, 247–322, doi:10.1002/2014RG000468.

Kneifel, S., P. Kollias, A. Battaglia, J. Leinonen, M. Maahn, H. Kalesse, and F. Tridon (2016), First observations of triple-frequency radar Doppler spectra in snowfall: Interpretation and applications, *Geophys. Res. Lett.*, *43*, 2225–2233, doi:10.1002/2015GL067618.

Knopf, D. A., P. A. Alpert, B. Wang, R. E. O'Brien, S. T. Kelly, A. Laskin, M. K. Gilles, and R. C. Moffet (2014), Microspectroscopic imaging and characterization of individually identified ice nucleating particles from a case field study, *J. Geophys. Res.*, *119*, 10,365–10,381, doi:10.1002/2014JD021866.

Koenig, L. R. (1963), The glaciating behavior of small cumulonimbus clouds, *J. Atmos. Sci.*, *20*(1), 29–47, doi:10.1175/1520-0469(1963)020 < 0029:TGBOSC>2.0.CO;2.
Lohmann, U., J. Humble, W. R. Leaitch, G. A. Isaac, and I. Gultepe (2001), Simulations of ice clouds during FIRE ACE using the CCCMA single-column model, *J. Geophys. Res.*, *106*(D14), 15,123–15,138, doi:10.1029/2000JD900473.
Milbrandt, J. A., and M. K. Yau (2005), A multimoment bulk microphysics parameterization. Part II: A proposed three-moment closure and scheme description, *J. Atmos. Sci.*, *62*, 3065–3081.
Morrison, H., and J. Milbrandt (2011), Comparison of two-moment bulk microphysics schemes in idealized supercell thunderstorm simulations, *Mon. Weather Rev.*, *139*(4), 1103–1130, doi:10.1175/2010MWR3433.1.
Morrison, H., J. A. Curry, and V. I. Khvorostyanov (2005), A new double-moment microphysics parameterization for application in cloud and climate models. Part I: Description, *J. Atmos. Sci.*, *62*, 1665–1677.
Murray, B. J., D. O'Sullivan, J. D. Atkinson, and M. E. Webb (2012), Ice nucleation by particles immersed in supercooled cloud droplets, *Chem. Soc. Rev.*, *41*, 6519–6554, doi:10.1039/C2CS35200A.
Niemand, M., et al. (2012), A particle-surface-area-based parameterization of immersion freezing on desert dust particles, *J. Atmos. Sci.*, *69*, 3077–3092, doi:10.1175/JAS-D-11-0249.1.
Paukert, M., and C. Hoose (2014), Modeling immersion freezing with aerosol-dependent prognostic ice nuclei in Arctic mixed-phase clouds, *J. Geophys. Res. Atmos.*, *119*, 9073–9092, doi:10.1002/2014JD021917.
Phillips, V. T. J., A. M. Blyth, P. R. A. Brown, T. W. Choularton, and J. Latham (2001), The glaciation of a cumulus cloud over New Mexico, *Q. J. R. Meteorol. Soc.*, *127*(575), 1513–1534, doi:10.1002/qj.49712757503.
Phillips, V. T. J., P. J. DeMott, and C. Andronache (2008), An empirical parameterization of heterogeneous ice nucleation for multiple chemical species of aerosol, *J. Atmos. Sci.*, *65*(9), 2757–2783.
Pruppacher, H. R., and J. D. Klett (1997), *Microphysics of Clouds and Precipitation, Atmos. Oceanogr. Sci. Libr.*, 2nd ed., Kluwer Academic, Dordrecht, Netherlands.
Rosenfeld, D., and W. L. Woodley (2000), Deep convective clouds with sustained supercooled liquid water down to −37.5°C, *Nature*, *405*(6785), 440–442, doi:10.1038/35013030.
Saleeby, S., and S. van den Heever (2013), Developments in the CSU-RAMS Aerosol Model: Emissions, nucleation, regeneration, deposition, and radiation, *J. Appl. Meteorol. Climatol.*, *52*(12), 2601–2622, doi:10.1175/JAMC-D-12-0312.1.
Segal, Y., and A. Khain (2006), Dependence of droplet concentration on aerosol conditions in different cloud types: Application to droplet concentration parameterization of aerosol conditions, *J. Geophys. Res.*, *111*, D15204, doi:10.1029/2005JD006561.
Seifert, A. (2008), On the parameterization of evaporation of raindrops as simulated by a one-dimensional rainshaft model, *J. Atmos. Sci.*, *65*(11), 3608–3619, doi:10.1175/2008JAS2586.1.
Seifert, A., and K. D. Beheng (2001), A double-moment parameterization for simulating autoconversion, accretion and selfcollection, *Atmos. Res.*, *59–60*, 265–281, doi:10.1016/S0169-8095(01)00126-0.
Seifert, A., and K. D. Beheng (2006), A two-moment cloud microphysics parameterization for mixed-phase clouds, Part 1: Model description, *Meteorol. Atmos. Phys.*, *92*(1–2), 45–66.
Seinfeld, J. H., and S. N. Pandis (2006), *Atmospheric Chemistry and Physics: From Air Pollution to Climate Change*, 2nd ed., John Wiley, Hoboken, N. J.
Simmel, M., and S. Wurzler (2006), Condensation and activation in sectional cloud microphysical models, *Atmos. Res.*, *80*(2–3), 218–236, doi:10.1016/j.atmosres.2005.08.002.
Simmel, M., T. Trautmann, and G. Tetzlaff (2002), Numerical solution of the stochastic collection equation—Comparison of the Linear Discrete Method with other methods, *Atmos. Res.*, *61*(2), 135–148, doi:10.1016/S0169-8095(01)00131-4.
Simmel, M., K. Diehl, and S. Wurzler (2005), Numerical simulation of the microphysics of an orographic cloud: Comparison with measurements and sensitivity studies, *Atmos. Environ.*, *39*(23–24), 4365–4373, doi:10.1016/j.atmosenv.2005.02.017.
Taylor, J. W., et al. (2016), Observations of cloud microphysics and ice formation during COPE, *Atmos. Chem. Phys.*, *16*(2), 799–826, doi:10.5194/acp-16-799-2016.
Tridon, F., and A. Battaglia (2015), Dual-frequency radar Doppler spectral retrieval of rain drop size distributions and entangled dynamics variables, *J. Geophys. Res. Atmos.*, *120*, 5585–5601, doi:10.1002/2014JD023023.
Ullrich, R., C. Hoose, O. Möhler, M. Niemand, R. Wagner, K. Höhler, N. Hiranuma, H. Saathoff, and T. Leisner (2017), A new ice nucleation active site parameterization for desert dust and soot, *J. Atmos. Sci.*, doi:10.1175/JAS-D-16-0074.1, in press.
Vali, G. (1971), Quantitative evaluation of experimental results on the heterogeneous freezing nucleation of supercooled liquids, *J. Atmos. Sci.*, *28*, 402–409.
Vali, G. (1994), Freezing rate due to heterogeneous nucleation, *J. Atmos. Sci.*, *51*(13), 1843–1856.
Vali, G. (2014), Interpretation of freezing nucleation experiments: Singular and stochastic; sites and surfaces, *Atmos. Chem. Phys.*, *14*(11), 5271–5294, doi:10.5194/acp-14-5271-2014.
Vali, G., and E. J. Stansbury (1966), Time-dependent characteristics of the heterogeneous nucleation of ice, *Can. J. Phys.*, *44*, 477–502.
Vogel, B., H. Vogel, D. Bäumer, M. Bangert, K. Lundgren, R. Rinke, and T. Stanelle (2009), The comprehensive model system COSMO-ART—Radiative impact of aerosol on the state of the atmosphere on the regional scale, *Atmos. Chem. Phys.*, *9*, 8661–8680.
Weisman, M. L., and J. B. Klemp (1982), The dependence of numerically simulated convective storms on vertical wind shear and buoyancy, *Mon. Weather Rev.*, *110*(6), 504–520, doi:10.1175/1520-0493(1982)110 < 0504:TDONSC>2.0.CO;2.
Welti, A., F. Lüönd, Z. A. Kanji, O. Stetzer, and U. Lohmann (2012), Time dependence of immersion freezing: An experimental study on size selected kaolinite particles, *Atmos. Chem. Phys.*, *12*(20), 9893–9907, doi:10.5194/acp-12-9893-2012.
Wisner, C., H. D. Orville, and C. Myers (1972), A numerical model of a hail-bearing cloud, *J. Atmos. Sci.*, *29*(6), 1160–1181, doi:10.1175/1520-0469(1972)029 < 1160:ANMOAH>2.0.CO;2.